The Aeronautical Journal (2026), 1–27
doi:10.1017/aer.2026.10240

RESEARCH ARTICLE

NO_x emission modelling for composite cycle engines with recirculation and water injection: A reduced-order physics-based approach

Fabio Witzgall, Gregory Uhl, Florian Winter, Yu-Hsuan Lin and Arne Seitz

Bauhaus Luftfahrt eV, Germany
Corresponding author: Fabio Witzgall; Email: fabio.witzgall@bauhaus-luftfahrt.net

Received: 27 February 2026 UTC; **Revised:** 18 August 2026 UTC; **Accepted:** 18 August 2026 UTC

Keywords: combustor; composite cycle engine; exhaust gas recirculation; free double piston; MINIMAL; NO reburn; NO_x emissions; NO_x mitigation; NO_x model; piston engine; stochastic flow model; two zone model; water injection

Abstract

The composite cycle engine (CCE) offers a promising pathway for significantly reducing fuel burn in future aircraft. By integrating a piston system into the core of a gas turbine, the CCE can utilise higher peak cycle temperatures and pressures and thus, achieve a step-change in thermal efficiency. These conditions also promote increased levels of NO_x formation. This paper presents a methodology for the preliminary estimation of NO_x emissions within both the piston engine and the subsequent Joule combustor. Fast-responding parametric models capable of capturing key NO_x sensitivities, particularly the impact of combustion vitiation through water injection and exhaust gas recirculation (EGR), are established. Piston NO_x is modelled using a two-zone approach, which demonstrates good correlation with reference engine data from literature. For the Joule combustor, a stochastic flow description is employed to predict NO_x formation, with validation against an in-service combustor confirming the model's predictive capability. Initial studies indicate high baseline piston NO_x emissions, though significant mitigation is achievable through water injection or EGR. This work establishes a framework for future research into the emissions and necessary mitigation strategies for the CCE and other advanced combustion technologies.

Nomenclature

List of symbols

A	two-zone temperature parameter
B	two-zone shape function
c	calibration parameter
d	diameter
EGR	exhaust gas recirculation rate
EI	emission index
FAR	fuel-air ratio
h	specific enthalpy
m	mass
M	molar mass
p	pressure
s	unmixedness
SFC	specific fuel consumption
t	time
T	temperature

© Bauhaus Luftfahrt e.V., 2026. Published by Cambridge University Press on behalf of Royal Aeronautical Society. This is an Open Access article, distributed under the terms of the Creative Commons Attribution-NonCommercial-NoDerivatives licence (https://creativecommons.org/licenses/by-nc-nd/4.0/), which permits non-commercial re-use, distribution, and reproduction in any medium, provided that no alterations are made and the original article is properly cited. The written permission of Cambridge University Press or the rights holder(s) must be obtained prior to any commercial use and/or adaptation of the article.

https://doi.org/10.1017/aer.2026.10240 Published online by Cambridge University Press

u	fluid velocity
v	piston velocity
w	mass flow
WAR	water–air ratio
α	combustor air addition profile
β	combustor primary zone air split
λ	air-excess ratio
ρ	density
σ	standard deviation
τ	timescale
ϕ	fuel-air equivalence ratio $= 1/\lambda$
φ	crank angle

List of subscripts/superscripts

0	initial / without combustion
1	combusted zone
2	uncombusted zone
3	combustor inlet
a	air
amb	ambient
$crit$	critical point
dil	dilution
EOC	end-of-combustion
f	fuel
inj	injected
mix	mixing / homogenisation
$stoich$	stoichiometric
SOC	start-of-combustion
w	water

List of acronyms

CCE	composite cycle engine
CFD	computational fluid dynamics
EGR	exhaust gas recirculation
EOC	end of combustion
FDP	free-double piston
LTO	landing & take-off operations
LR	long-range
PSR	perfectly stirred reactor
PDF	probability density function
RQL	Rich-burn, quick-mix, lean-burn
SLS	sea-level static
SAF	sustainable aviation fuel

1.0 Introduction

Future propulsion concepts are driven by the need to significantly reduce the climate impact of aviation, while ensuring low fuel consumption for airlines to stay competitive. Among several novel candidates, the composite cycle engine (CCE) concept has been investigated for several years [1, 2]. This concept introduces a piston engine system to the core of a gas turbine engine. While various CCE architectures in both two- and four-stroke configurations, including reciprocating, rotary and free-piston variants, have been investigated, this work is motivated by the so-called free-double piston (FDP) variant. This architecture is of particular interest for its potential lower mass, as it functions strictly as

https://doi.org/10.1017/aer.2026.10240 Published online by Cambridge University Press

a gas generator without mechanical power provision, utilising an integrated unit of piston compressors and opposite-located engine cylinders that share a single piston element. The FDP solution was first described by Klingels [3], with a detailed description and its conceptual design implications initially presented by Kaiser et al. [4].

The closed-volume combustion of the piston engine, as well as the higher cycle peak temperatures and pressures, results in significant improvements in thermal efficiency [1]. When integrated and assessed at the aircraft level, the thermal efficiency benefits translate to healthy double-digit mission fuel burn reductions relative to similarly advanced geared turbofan engines. However, these benefits are accompanied by an increase in system weight and NO_x emissions. As the piston engine is responsible for the bulk of CCE NO_x emissions due to elevated temperatures and pressures, addressing this source is particularly critical for the viability of the concept. As shown by Kaiser et al. [5], CAEP/6-75% targets are projected to be exceeded by the CCE, with cruise-phase emissions being of particular concern due to their disproportionate impact on climate. Effective NO_x mitigation measures are therefore crucial.

Mitigation strategies under consideration include optimisation of valve and injection timings, compression intercooling ahead of the piston system, relocation of fuel injection to the Joule combustor (at the expense of thermal efficiency), application of rich combustion in the piston stage with lean combustion in the Joule combustor (with potential soot formation and high cylinder temperatures) and combustion vitiation (e.g. by gas recirculation or water injection) [4]. All approaches involve engine- and aircraft-level trade-offs. Exhaust gas recirculation (EGR) and water injection have shown particularly high NO_x reduction potential, as they simultaneously reduce flame temperature and oxygen availability for emission formation. Due to their promising potential in both piston and gas turbine systems [6–8], the impact on NO_x emissions in the CCE is further investigated in this paper.

Nitrogen oxides (NO_x) emitted from internal combustion engines and gas turbines consist primarily of nitric oxide (NO) and nitrogen dioxide (NO_2). While multiple formation pathways exist, including the prompt, N_2O and NNH mechanisms relevant for hydrocarbon-rich, lean-low-temperature or high-pressure, or hydrogen-combustion regimes, respectively [9, 10], the high-temperature environment of the CCE establishes the thermal NO (extended Zeldovich) mechanism as the dominant contributor. Fuel-bound nitrogen and its NO formation path is negligible for standard aviation fuels [10]. Furthermore, while the high inlet NO concentrations in the CCE Joule combustor suggest potential for NO reburning, a reduction phenomenon observed in vitiated flows that requires more detailed chemistry [11–13], this study adopts a simplified approach by focusing on the gross production via the thermal route. Consequently, the modelling effort is centred on the extended Zeldovich mechanism.

The estimation of NO_x formation requires precise knowledge of local temperatures and species concentrations. The scientific literature categorises the modelling efforts into a hierarchy based on spatial resolution and computational effort. At the highest level of complexity, 3D computational fluid dynamics (CFD) models provide high-fidelity spatial resolution by solving the Navier–Stokes equations, capturing the detailed interaction between turbulent flow, spray evaporation and local chemical kinetics. However, the long computation times required make CFD inadequate for early predesign, which requires estimates over wide parameter sweep studies. Conversely, global correlation-based models, widely used for their simplicity, link global parameters such as inlet conditions and fuel-air ratio (*FAR*) to experimental datasets. While effective for derivative engines within their calibration range, these models often lack the physical predictive capability required for novel architectures. This is particularly true for piston engines, where the high number of sensitive parameters limits the applicability of simple correlations. To bridge this gap between complexity and utility, quasi-dimensional models have been deployed, segmenting the combustion process into discrete volumes or zones while retaining a physically based representation of the dominant processes. By simulating the thermodynamic history of individual zones, these models capture the local variations in *FAR* that drive NO_x formation. While multi-zone approaches offer high fidelity in piston engines, they require detailed input data, such as injection rate profiles and spray geometry [14–16]. Consequently, there is a need for a balanced modelling approach that captures the essential physics of peak temperatures. This is crucial for both piston and Joule combustors, while maintaining the computational efficiency required for system-level studies for the CCE.

https://doi.org/10.1017/aer.2026.10240 Published online by Cambridge University Press

This work presents a quasi-dimensional modelling framework for both the piston engine and the Joule combustor, designed to bridge the gap between empirical correlations and high-fidelity simulations. The methodology is demonstrated through studies of NO_x emission in an FDP-CCE, with a particular focus on water injection and EGR. Although the proposed methodology is inherently fuel-agnostic, this work focuses primarily on kerosene-based applications. Additionally, its versatility is demonstrated through a piston engine validation case involving hydrogen (H2).

2.0 Methodology

2.1. NO_x *kinetics*

This study only considers thermal NO formation described by the extended Zeldovich mechanism [9]:

$$N_2 + O \overset{k_1}{\longleftrightarrow} NO + N \tag{1}$$

$$N + O_2 \overset{k_2}{\longleftrightarrow} NO + O \tag{2}$$

$$N + OH \overset{k_3}{\longleftrightarrow} NO + H \tag{3}$$

The available concentrations of species N, O and OH at the respective fluid composition and temperature are determined with the OHC-system. The implementation of the extended Zeldovich and the OHC-system, including the determination of the forward and backward reaction rates k_{1-3} and validation, is described by Kaiser [17].

While NO is the primary species formed and emitted at the engine exhaust, it is unstable in the atmosphere. Over time, practically all exhaust NO oxidises to form nitrogen dioxide (NO_2). Because of this inevitable conversion, environmental regulations standardise the reporting of NO_x emissions. Regardless of the actual ratio of NO to NO_2 at the tailpipe, the total mass of NO_x is calculated using the molar mass of NO_2 [18]:

$$m_{NO_x} = n_{NO} \cdot M_{NO_2} \tag{4}$$

The NO_x mass results from the number of NO moles n_{NO} and the molar mass $M_{NO_2} = 46.0055\ g/mol$. The NO_x results in this work are given with the emission index, which relates NO_x mass to fuel burn mass as $EI\ NO_x = m_{NO_x}/m_f$.

2.2. Piston NO_x *model*

The piston system is modelled in an in-house tool, capable of calculating different types of piston compressors and engines. This includes the performance calculation and the NO_x emissions calculations, whereas the latter is estimated as a post-processing step.

For the performance calculation, the piston engine is described by a zero-dimensional, single-zone model, resolving the thermodynamic performance in timesteps, commonly defined by crank angle for one full revolution of the cycle. The combustion process is described with the empirical Wiebe function, where two Wiebe parameters (w_a and w_m) are applied to describe the heat release rate [19]. The w_a parameter defines the fuel burn utilisation. In the default setup, w_a is set to 6.908 for lean combustion, representing 99.9% of combustion efficiency. In the present predesign study, w_a is kept constant for lean operating points, which assumes stable and nearly complete combustion. This is considered appropriate for the investigated operating range, but may become optimistic for very lean mixtures, where incomplete combustion or combustion instability effects could reduce the actual fuel-burn utilisation. For a rich, oxygen-limited operation, w_a is reduced according to the availability of oxygen. For the heat transfer from the hot gas to the cylinder wall, several semi-empirical models were tested and calibrated with the crankshaft-based engine described by Van Gerpen [20]. After comparison of the overall performance and main cycle parameter evolutions, the correlation given by Hohenberg [21] is selected, as it best matches the overall piston engine performance. A calibration factor of 0.64 is applied to the Hohenberg heat-transfer model to best reproduce the reference engine performance. Since the correlation does

https://doi.org/10.1017/aer.2026.10240 Published online by Cambridge University Press

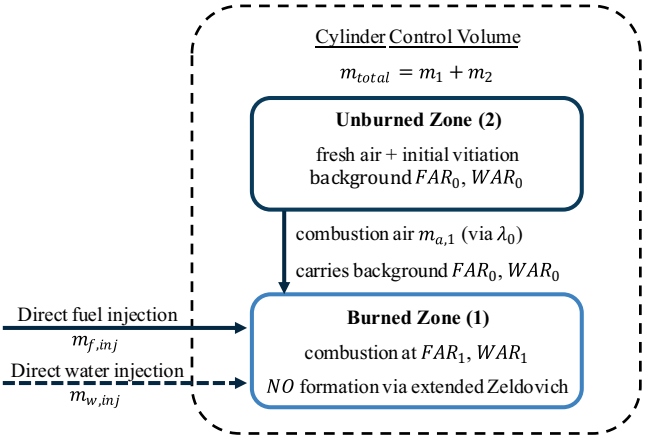


Figure 1. *Schematic of the two-zone mass balance.*

not explicitly account for high-wall-temperature heat transfer effects, their influence on the predicted cylinder-temperature history remains a modelling uncertainty. Neglecting such effects is expected to be conservative with respect to thermal NO formation, as enhanced wall heat transfer would tend to lower peak gas temperatures. For more details on the piston system modelling, the reader is referred to Kaiser [17] and Lin et al. [22]. Analogous modelling for hydrogen fuel has been described by Nickl et al. [23] and Winter et al. [24]. Due to the absence of soot in hydrogen combustion, which acts as an insulator in internal combustion engines, a modified Woschni correlation [25] is used with a calibration factor of 3.3 to reflect this phenomenon. In addition, the combustion duration is shortened compared with the kerosene variant to represent the shorter combustion times associated with hydrogen operation.

2.2.1. Model description

Single-zone models capture only the mean cylinder temperature and composition and are thereby insufficient to describe hot cylinder regions that are crucial for NO_x formation. In contrast to multi-zone models, the two-zone approach simplifies the combustion chamber into two distinct thermodynamic domains: the unburned and the burned (combusted) zones. These regions are separated by an infinitely thin flame front, which is typically not explicitly modelled due to its negligible volume and limited direct impact on the global kinetics of NO formation.

The primary differentiation among two-zone methodologies lies in their initialisation of these domains and the mechanisms used to describe their interaction. Li et al. [26] present a two-zone reaction-based combustion model that accounts for both heat and mass exchange between the zones. The model described by Kozuch [27] includes a detailed mixing model, solving a global homogeneous isotropic $k-\epsilon$ model to resolve cylinder turbulence. Similar approaches to calculate in-cylinder turbulence to determine mixing are given by Andersson et al. [28] and Brückner et al. [29]. Heider et al. [30] instead describe a more empirical two-zone model that only requires few engine-specific input parameters. Oppenauer and Del Re [31] combine the Heider approach with the parallel mixing model of Kozuch [27]. The authors also highlight that pure physical models are difficult to adapt, especially to modern diesel engines, as the required calibration parameters vary during operation.

In the following, the two-zone model implementation is described, as it proved sufficiently accurate while requiring a minimum amount of unknown setup parameters. The fundamental logic originates from Heider et al. [30], with the implementation most closely resembling Kaiser [17].

Figure 1 visualises the two-zone mass balance, which is described in mathematical terms through Equations (5–9). The cylinder mass is partitioned into a burned (1) and unburned zone (2),

$$m_{total} = m_1 + m_2, \tag{5}$$

https://doi.org/10.1017/aer.2026.10240 Published online by Cambridge University Press

where m_1 and m_2 are the two zone masses. The fuel-air ratio of the burned zone FAR_1 is defined by the air-excess ratio λ_0 and the stoichiometric FAR_{stoich}:

$$FAR_1 = \frac{FAR_{stoich}}{\lambda_0} \tag{6}$$

The effect of vitiated inlet air and incomplete scavenging is represented through background fuel and water contents in the incoming charge. These background quantities define the initial FAR_0 and WAR_0, which are constant across both zones. Directly injected fuel $m_{f,inj} = m_f - m_{f,0}$ and water $m_{w,inj} = m_w - m_{w,0}$ are added only to the combusted zone, resulting in the burned zone composition FAR_1 and WAR_1. Consequently, a change in FAR_0 alone does not alter FAR_1; instead, the amount of freshly burned fuel and the corresponding heat release are determined by the difference $FAR_1 - FAR_0$. This difference defines the air mass $m_{a,1}$ participating in combustion.

$$m_{a,1} = \frac{m_{f,inj}}{FAR_1 - FAR_0} \tag{7}$$

$$WAR_1 = \frac{m_{w,inj}}{m_{a,1}} + WAR_0 \tag{8}$$

$$m_1 = m_{a,1} \cdot (1 + FAR_1 + WAR_1) \tag{9}$$

Heider et al. [30] give a simple model for the temperature difference between the burned and unburned zones.

$$T_1 - T_2 = B(\varphi) \cdot A \tag{10}$$

The shape function $B(\varphi)$ describes the evolution of the temperature difference along the crank angle φ and gives an estimate for the energy interaction between the two zones based on pressure evolution,

$$B(\varphi) = 1 - \frac{\int_{\varphi_{SOC}}^{\varphi} (p(\varphi) - p_0(\varphi))\, m_1(\varphi)\, d\varphi}{\int_{\varphi_{SOC}}^{\varphi_{EOC}} (p(\varphi) - p_0(\varphi))\, m_1(\varphi)\, d\varphi}, \tag{11}$$

with $p(\varphi)$ being the cylinder pressure and $p_0(\varphi)$ the pressure without combustion. SOC and EOC refer to start and end of combustion.

The factor A is described by Heider et al. [30] as an engine-specific calibration temperature difference. Oppenauer and Del Re [31] extend A to be variable with swirl and EGR. Kaiser [17] describes the same approach as chosen here, where A is defined as a temperature difference based on the adiabatic flame temperature.

$$A = c_A\,(T_{flame} - T_{SOC}) \tag{12}$$

The adiabatic flame temperature T_{flame} is established via an enthalpy balance between SOC conditions and the flame conditions given by FAR_1, WAR_1 and the water injection temperature $T_{w,inj}$. Compared with the original Heider formulation, this definition reduces the calibration burden on c_A, since the temperature difference $T_{flame} - T_{SOC}$ already accounts for changes in mixture composition, vitiation, water addition and SOC thermodynamic conditions.

To calculate the zone temperatures, an enthalpy balance ensures energy conservation,

$$m_{total}\, h_{total} = m_1\, h_1 + m_2\, h_2, \tag{13}$$

with the specific enthalpies h resulting from the temperature, pressure and composition in the zones.

2.2.2. Calibration and validation

The described methodology results in two calibration parameters. The air-excess ratio λ_0 captures the amount of air added to the burned zone, with $\lambda_0 = 1$ describing stoichiometric combustion. An increase of λ_0 will initially result in an increase in NO as the increased availability of oxygen outweighs the

https://doi.org/10.1017/aer.2026.10240 Published online by Cambridge University Press

Table 1. *Overview of piston engine setups used for validation*

Engine	Stroke	Bore [m]	λ_0	c_A
Diesel MAN B&W 4T50ME [1]	2	0.5	1.093	0.9
Diesel Large Generator [2]	2	0.58	1.060	0.9
H_2 Lombardini 15LD500 [3]	4	0.087	1.005	0.9

[1] [6, 15, 33].
[2] [14].
[3] [34, 35].

decrease in flame temperature. As λ_0 moves further away from stoichiometric conditions, the predictive capability of a single representative value decreases since in a real engine, NO formation is governed by a distribution of local equivalence ratios, temperatures and radical concentrations rather than by a spatially uniform-burned zone composition. Rich and lean regions will differently impact NO formation due to the availability of radicals. For direct injection, a single λ_0 near stoichiometry has been shown to be capable of providing a good NO estimate. For premixed conditions, the predictions will be less accurate.

The parameter c_A scales the initial zone temperature difference, with $c_A = 1$ resulting in $T_1(\varphi_{SOC}) = T_{flame}$. Brückner et al. [29] found that actual peak temperatures in conventional diesel combustion typically remain approximately 150 K below the adiabatic flame temperature. However, the authors also find that peak temperatures approach or even surpass this limit in premixed-dominated regimes. This convergence is primarily driven by reduced mixing rates and the compression heating of post-flame gases, which counteracts the thermal dissipation typically seen in diffusion flames. Andreasen and Mayer [32] reduce the calculated flame temperature by approx 100 K via heat radiation. During validation $c_A = 0.9$ was found to result in decent NO_x trends while the resulting reduction in A matched the above-cited temperature ranges.

While in this study c_A was kept constant, one could make a case to modify it for a reason other than simply the difference between adiabatic flame temperature and actual hot gas temperature. Although the Heider two-zone model accounts for inter-zone energy transfer via the shape function B (Equation 11), it does not explicitly resolve the finite-rate turbulent mixing or local mixture stratification. Under high-pressure, high-temperature conditions close to stoichiometry, NO formation may therefore approach equilibrium rapidly. In such cases, the simplified treatment of mixing and stratification may cause the calculated NO concentration to become limited by equilibrium during the peak-temperature period. Consequently, λ_0 is typically adjusted empirically to match experimental NO results. While this may suffice for part-load studies, it can result in an underestimation of NO_x reduction when evaluating advanced mitigation strategies, such as water injection. In such cases, the model may fail to show the expected NO reduction from flame temperature cooling because the predicted concentrations initially remain equilibrium-limited. As c_A directly affects peak temperature, it could be used as a proxy in calibration to limit the extent to which NO formation becomes equilibrium-controlled. In the present study, however, it is kept constant, as satisfactory agreement with literature data was obtained and, given the uncertainty inherent to predesign studies, a physically well-founded justification for its adjustment would be difficult.

The chosen validation engines and calibration parameters are presented in Table 1. To validate the described piston NO_x model, crankshaft-based engines have been set up due to the lack of sufficiently detailed data on free piston engines. The performance setups were tuned to closely align with available data, such as temperature or pressure evolutions and integral metrics such as power or specific fuel consumption SFC. Subsequently, λ_0 was tuned for best alignment with literature data, while c_A was kept constant. In addition to the diesel part-load studies, previously shown by Kaiser [17], an H2 engine and vitiated air studies were added.

Figure 2 shows the load and EGR (at 75 % load) study for the MAN B&W 4T50ME-X. The model captures the power-specific NO_x emissions well across various loads. However, an underestimation of specific emissions decrease with increasing load can be observed. This decrease is likely a result of the improved mixing at higher engine speeds, which is not captured by the model. For the EGR study, the

https://doi.org/10.1017/aer.2026.10240 Published online by Cambridge University Press

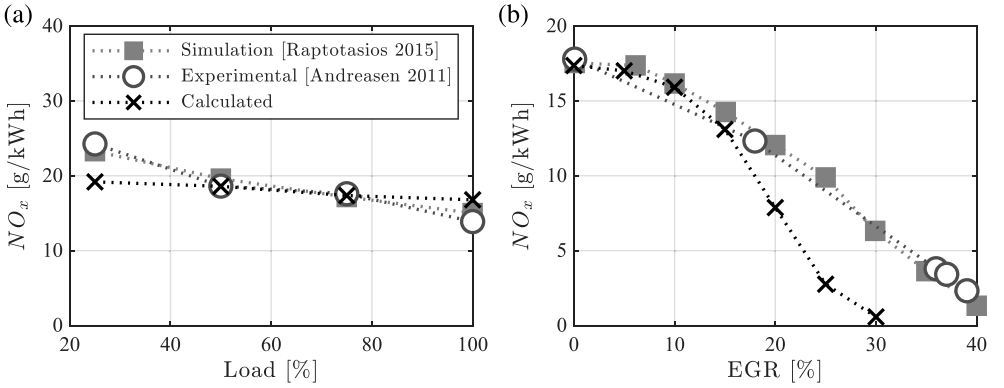


Figure 2. NO_x *predictions for the MAN B&W 4T50ME-X (a) load and (b) EGR study.*

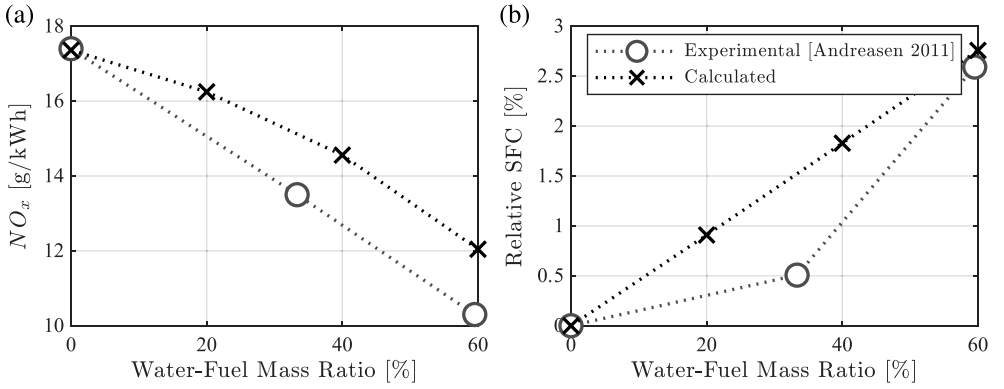


Figure 3. NO_x *and SFC predictions for the MAN B&W 4T50ME-X water-in-fuel emulsion study.*

inlet *FAR* was calculated for each *EGR* value on a dry volume basis, as described by Andreasen and Nyggard [6]. The model captures the trend generally well, with the exception of high *EGR* values. The experimental setup utilised an exhaust gas scrubber that cools the recirculated air and removes significant amounts of water, resulting in dry EGR. Because the *FAR* definition of the model inherently includes combustion-product water, it cannot currently simulate a fully dry recirculation path. This is the likely reason for the higher emission reduction predicted with *EGR*, where the additional increase in specific heat capacity of the recirculated water has a substantial effect on the flame temperature and thereby NO formation. For the aeronautical application only wet EGR will be considered.

Figure 3a shows the NO_x emission predictions for the MAN B&W 4T50ME-X operating with water-in-fuel emulsion at 75 % load. In contrast to the experiment, water is not premixed with the fuel in the model; instead, it is introduced into the cylinder at 298.15 K, with the mass flow determined by the fuel flow and the specified water-fuel ratio (*WFR*). The model predicts a linear increase in specific fuel consumption (*SFC*) due to the thermodynamic penalty of heating the water to cylinder temperatures and the associated latent heat of vaporisation (Figure 3b). The experimental results [6] show a less pronounced *SFC* increase at moderate *WFR* and even report *SFC* improvements at lower loads. The authors suggest this effect could result from an effective fuel nozzle optimisation due to the added mass flow. At low *WFR*, the model predicts a gradual NO_x reduction, highlighting the sensitivity of the model to the transition between equilibrium-controlled and kinetically limited NO formation. At higher *WFR*, NO formation becomes clearly kinetically limited, and the model's predicted reduction slope closely matches the experimental trends.

https://doi.org/10.1017/aer.2026.10240 Published online by Cambridge University Press

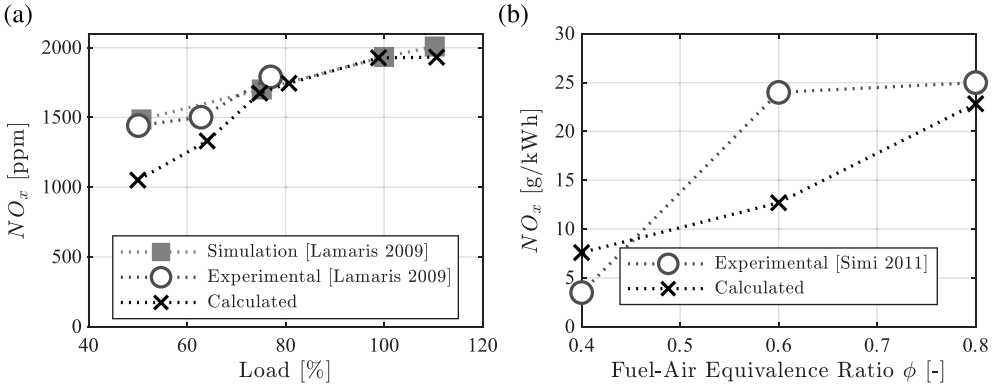


Figure 4. NO_x *prediction for (a) the large generator load study [14] and (b)* H_2 *4-stroke Lombardini 15LD500 [35].*

Figure 4a depicts the load study of the large diesel generator described by Lamaris et al. [14]. The model shows good alignment at high load but underestimates the NO_x emissions at lower load. For the small H_2 engine at 2500 rpm shown in Figure 4b, the model captures the trend of increasing NO_x emissions with equivalence ratio but fails to capture the high emissions for $\phi = 0.6$. Sfriso et al. [34] show that the early injections in this engine result in a wide distribution of local equivalence ratio. The distributions change with global ϕ and engine speed. For $\phi = 0.6$ at high engine speed, the local equivalence ratios reach up to stoichiometry. This shows one limitation of the model, where the single equivalence ratio choice for the combusted zone fails to capture the wide distribution of the actual conditions.

Overall, the piston NO_x model shows to be capable of predicting general NO_x trends in the studied piston engines well, including water injection and EGR. For the large two-stroke diesel engines, good alignment with a higher λ_0 of 1.06 and 1.093 was found. These result in a higher NO_x than at the stoichiometric setting due to air entrainment. However, the small four-stroke H_2 engine calibration resulted in a near-stoichiometric combusted zone with $\lambda_0 = 1.005$. The previous application of this two-zone model [17] showed two smaller four-stroke engines with λ_0 at 1.01 and 1.03. While these ranges might imply a dependency on the engine cycle (two-stroke vs. four-stroke), here it is argued that engine scale and speed are the more physically relevant factors. In large-bore engines, larger physical mixing scales and slower speeds favour a broader, leaner bulk NO_x production zone. Conversely, in small-bore engines, regardless of cycle architecture, rapid mixing tends to restrict high-temperature NO_x production to narrow, near-stoichiometric interfaces.

Consequently, for the smaller-bore two-stroke FDP engine evaluated in this study, $\lambda_0 = 1$ is adopted. This choice prioritises the physical similarities in mixing dynamics with small four-stroke engines over the nominal similarity in cycle architecture with large diesel engines. While this hypothesis provides a consistent physical basis for this study, further validation, preferably with a two-stroke, small-bore, free-piston engine, is recommended. Within the defined scope, the model is considered sufficient to capture the general trends in the investigated CCE.

2.3. Joule combustor NO_x *model*

2.3.1. Model description

Similar to the piston engine, the fundamental difficulty of gas turbine NO_x modelling lies in the extreme temperature sensitivity of the thermal NO mechanism. The rate of formation scales exponentially with temperature; consequently, the majority of NO is produced in local regions where the equivalence ratio is near stoichiometric ($\phi \approx 1$), even if the global mixture is lean. Traditional zero-dimensional (0D) models that assume a perfectly stirred reactor (PSR) based on average inlet conditions often fail to capture this reality. They tend to substantially underpredict NO formation at lean operating points.

https://doi.org/10.1017/aer.2026.10240 Published online by Cambridge University Press

To resolve the combustor mixture without solving the 3D Navier–Stokes equations, stochastic descriptions of the flow field have been introduced [36, 37]. This methodology assumes that while the spatial location of a fuel pocket is unknown (0D/1D approximation), the probability of finding a fluid element at a specific equivalence ratio can be mathematically defined. The key aspects for these models are the stochastic description of the local equivalence ratio and its time evolution.

The stochastic distribution of the local equivalence ratio (ϕ) can be described by a probability density function (PDF). Heywood and Mikus [37] assume a Gaussian distribution, while other distributions such as β-PDFs could offer more flexibility if supporting data is available. Heywood and Mikus also consider the stochastic distribution of the local residence time in the primary zone. The fluid homogenises with time, which is of key interest to NO_x formation. This can be captured by sectioning of the combustion chamber into zones with different roles. Heywood and Mikus [37] consider a primary zone without any mixing and a secondary zone where cooling air dilutes the richer primary zone gases and quickly freezes the NO formation process. Therefore they only consider primary zone formation, while noting that this assumption fails if a substantial part of the primary zone flow is fuel rich. Fletcher and Heywood [36] consider an intermediate zone after the primary zone where homogenisation of the standard deviation takes place proportional to $\sqrt{t}$. In the following dilution zone no further NO formation is assumed. Dederichs et al. [38] assume an exponential decrease of the standard deviation with respect to a characteristic time, which was established by means of a reacting large eddy simulation (LES).

The strength of such a stochastic approach is its ability to decouple the macro-scale fluid dynamics from the micro-scale mixing and describing these with a limited number of physical parameters. The assumed PDF can easily be modified to allow for more control over the flow mixedness. This allows quick calibration to different combustor designs, while keeping computational costs low. However, no description for an appropriate cooling air addition model, which is critical to e.g. rich-burn, quick-mix, lean-burn (RQL) combustors, was found in the literature. In the following an implementation for such a stochastic model is described, including the novel adaption to RQL-type combustors. The foundational model could also be adapted to other advanced combustion concepts, such as lean direct injection or staged combustion, which would be an interesting area for future research.

This model simplifies the spatial considerations by assuming only one zone with both homogenisation of the mixture and mixing with the cooling air. To account for the imperfect mixing of fuel and air, the methodology employs a Gaussian (normal) PDF to describe the distribution of local equivalence ratio ϕ within the combustor, following the description by Heywood and Mikus [37],

$$f(\phi) = \frac{1}{\sigma\sqrt{2\pi}} \cdot exp\left[-\frac{(\phi - \bar{\phi})^2}{2\sigma^2}\right], \tag{14}$$

where σ is the standard deviation. The mixing quality is quantified by the unmixedness parameter s, defined as the ratio of the standard deviation σ to the mean equivalence ratio $\bar{\phi}$:

$$s = \frac{\sigma}{\bar{\phi}} \tag{15}$$

The evolution of mixture inhomogeneity is modelled as an exponential decay, described by a characteristic mixing timescale τ_{mix} and the initial unmixedness s_0 [38]:

$$s(t) = s_0 \cdot exp\left(-\frac{t}{\tau_{mix}}\right) \tag{16}$$

The mean equivalence ratio $\bar{\phi}$ is determined by the injected fuel mass and the cumulative air addition profile $\alpha(t)$. Only a part of the inlet air is directly routed into the primary zone. This split is described by the assumed inlet air split β:

$$\beta = \frac{w_{t=0}}{w_{inlet}} \tag{17}$$

Here, $w_{t=0}$ refers to the mass flow in the combustor at start of simulation and w_{inlet} is the inlet mass flow from the upstream component.

https://doi.org/10.1017/aer.2026.10240 Published online by Cambridge University Press

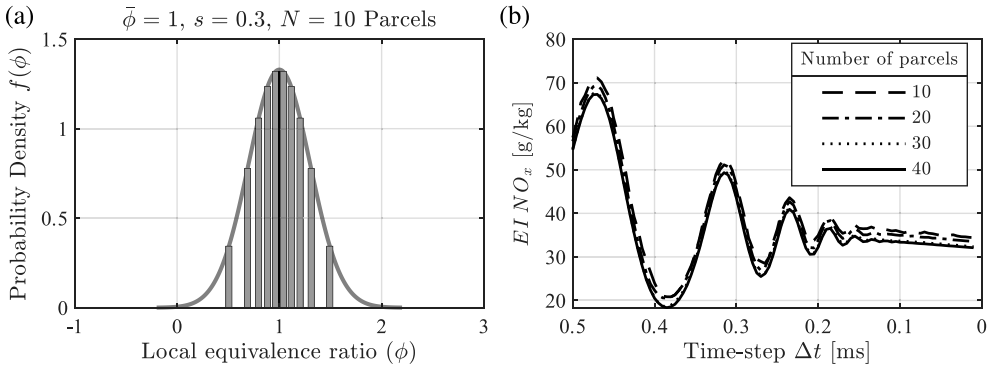


Figure 5. *Joule combustor* NO_x *model (a) discretisation visualisation and (b) discretisation sensitivity.*

To capture the quick quenching required in RQL combustors, the cooling air dilution is modelled with a squared exponential based on a characteristic dilution timescale τ_{dil}. This phenomenological formulation assumes all cooling air to be added within this quick mixing. In real combustors a substantial fraction of the cooling air is added continuously for dilution towards the combustor exit, but the assumption is made that this has little influence on NO formation, as it is frozen by the quenching. The cumulative air addition profile α at time t is defined as

$$\alpha(t) = \begin{cases} \beta & \text{for } 0 \leq t \leq \tau_{primary} \\ \beta + (1-\beta) \cdot \left(1 - exp\left[-\left(\frac{t - \tau_{primary}}{\tau_{dil}}\right)^2\right]\right) & \text{for } t > \tau_{primary} \end{cases}, \tag{18}$$

with $\tau_{primary}$ describing the length of the rich, primary zone ahead of quenching.

The dilution τ_{dil}, the mixing timescale τ_{mix} and the primary zone time $\tau_{primary}$ are dependent on engine operation. As done by Dederichs et al. [38], the timescales are estimated with calibration parameters c_{dil}, c_{mix} or $c_{primary}$, the bulk flow velocity u_{bulk} and a characteristic length (here the nozzle diameter is used).

$$\tau_i = c_i \frac{d_{nozzle}}{u_{bulk}} = c_i \frac{\rho\, A_{combustor}\, d_{nozzle}}{\dot{m}} \tag{19}$$

$A_{combustor}$ refers to the annular cone flow area after the injector including the cooling ducts. The nozzle diameter d_{nozzle} serves as a characteristic diameter for the premixing passage.

2.3.2. Discretisation

The flow field is discretised both temporally and stochastically with respect to the local fuel–air equivalence ratio ϕ. The stochastic discretisation segments the PDF given by Equation (14) into a set of parcels, with each parcel representing the same fixed fraction of the fuel mass flow (see Figure 5a). The respective air mass then results from the local ϕ obtained from the inverse cumulative distribution function of $f(\phi)$. Total mass conservation is ensured through appropriately scaled parcels.

The discretisation sensitivity is displayed in Figure 5b. Noteworthy is the high sensitivity to the timestep highlighting the time-sensitive nature of thermal NO formation. The number of parcels is less impactful on NO_x with little difference between 30 and 40 parcels. Accordingly 30 parcels and timestep intervals of 0.1 ms are selected as they lie within 4% of the highest-resolved setting while minimising computational cost. Due to the sensitive calibration, this deviation is secondary. Calculation times are then typically well within a second.

The temperature in each parcel and timestep is calculated from a flame temperature calculation via enthalpy balance to inlet conditions given the local ϕ. Effects of vitiated air, as in the case of the

https://doi.org/10.1017/aer.2026.10240 Published online by Cambridge University Press

precombusted air in the CCE, are captured by the inlet conditions, which propagate into the combustor. The thermal NO formation at each timestep and parcel is calculated as previously described in subsection 2.1.

2.3.3. Calibration and validation

The proposed model integrates outputs from a gas turbine performance simulation as primary boundary conditions. Specifically, it requires the inlet mass flow, pressure, temperature, *FAR* and water–air ratio (*WAR*), alongside the total fuel mass added. Furthermore, the chemical and mixing evolution within the combustor is defined by a number of parameters: the inlet air split β, representing the initial equivalence ratio; the initial unmixedness s_0; and the characteristic timescales for internal homogenisation τ_{mix}, dilution τ_{dil} and the primary zone $\tau_{primary}$. While these timescales are derived from specific calibration constants, as described by Equation (19), their physical significance and representative values from the literature are discussed in the following section.

The inlet air split β represents the fraction of total combustor air directed into the primary reaction zone. It establishes the initial stoichiometry, dictating the base level of thermal NO production before any secondary dilution or internal mixing occurs and whether later the stoichiometric region needs to be crossed. The upper bound of β is typically constrained by the lean flammability limit. In staged combustion systems, a lightly loaded primary zone may operate at an equivalence ratio of approximately 0.8 during low-power conditions to ensure high combustion efficiency and minimise CO and unburned hydrocarbon (UHC) emissions. Conversely, at full-load conditions, the primary zone ϕ is often lower, at around 0.6, to mitigate NO_x formation as the secondary zone becomes active ([39], pp. 24–25). RQL combustors show an even higher initial equivalence ratio (1.2–1.6 [39]) and rely on quick mixing. Smith [40] reports a primary zone equivalence ratio of about 2 for the V2500-A5 combustor at 100% load, with only 19% and 7% of total combustor air going to the primary zone and the nozzle, respectively. It was found that such rich primary zones would typically result in $\beta < 0.4$.

The unmixedness s_0 accounts for the spatial fluctuations in the fuel-air mixture. Due to the exponential dependence of thermal NO_x formation on temperature, local hot spots near stoichiometric regions produce significantly higher emissions than a perfectly homogeneous mixture at an identical mean temperature. Consequently, s_0 is essential for capturing the influence of these high-temperature eddies. The impact of initial unmixedness is fundamentally coupled with the mean equivalence ratio and, by extension, the air split β. While a lower limit of $s_0 = 0$ represents a perfectly premixed state, which is difficult to achieve in aero-engine combustors, higher values characterise non-premixed systems. For instance, Heywood and Mikus [37] used $s_0 = 0.5$ for predicting GT-309 NO emissions ($\phi(t = 0) = 0.81$ at 100% load). Smith [40] reported s_0 in the range of 0.2 to 0.4 for rich Pratt & Whitney injectors. Smith identified two primary drivers for mixing quality: the injection mechanism and the total energy available for mixing, typically represented by the pressure drop across the combustor. It is expected that unmixedness increases as engine load decreases, as both the turbulence intensity from the fuel injectors and the available pressure drop are reduced.

The mixing timescale τ_{mix} represents the time required for fuel and air to reach a homogeneous state. Heywood and Mikus [37] assume no change in umixedness with time, as they consider a stochastic distribution of the primary zone residence time. Dederichs et al. [38] estimated a characteristic mixing time of 5.03 ms, while noting lower numbers from the literature. Beyond direct estimation, τ_{mix} (in conjunction with s_0) can be calibrated by evaluating species or temperature distributions at the combustor exit plane. These distributions are frequently documented in literature due to their critical influence on high-pressure turbine cooling requirements and nozzle guide vane durability. Alternatively, as a first-order approximation, the timescale may be estimated using the geometric combustor length and the bulk average flow velocity.

The dilution timescale τ_{dil} defines the rate at which secondary air is introduced. In RQL architectures, rapid dilution is critical for minimising residence time within the high NO_x window, where fuel-rich pockets inevitably pass through stoichiometric conditions before reaching the final lean state.

https://doi.org/10.1017/aer.2026.10240 Published online by Cambridge University Press

Table 2. *Model setup for the V2533-A5 RQL combustor*

Variable	Unit	Value	Justification
β	–	0.22	Primary zone $\bar{\phi} = 2$ at 100% thrust and within primary zone massflow fraction range [47].
s_0	–	0.3	Mean of 0.2 – 0.4 [40], as not modified in partload.
c_{mix}	–	5	As reported by Ref. [38]. Due to the early quenching the homogenisation timescale is secondary.
c_{dil}	–	0.24	Main calibration parameter, as quenching timescale most impactful on final NO_x.
$c_{primary}$	–	0.5	Chosen for the 30% thrust point, as it is near stoichiometric in the primary zone.
d_{nozzle}	m	0.03	Measured from V2500 drawing.
$A_{combustor}$	m^2	0.35	Measured from V2500 drawing.

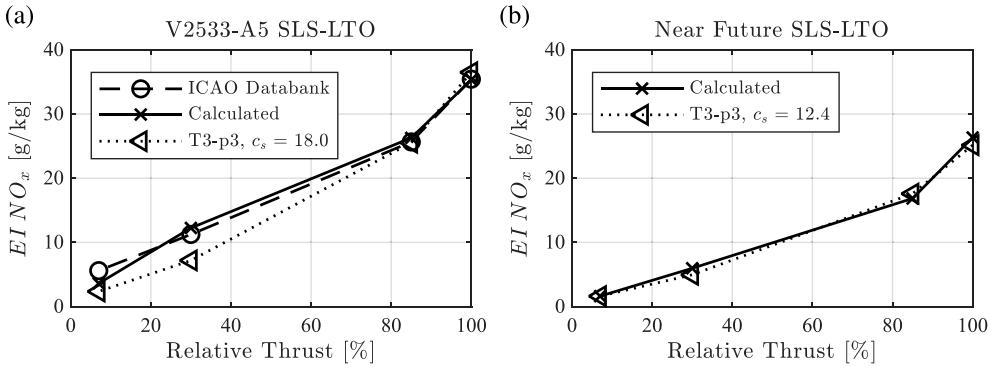


Figure 6. *Sea-level static LTO cycle* NO_x *prediction of the (a) V2533-A5 compared to ICAO databank and (b) near future setup.*

Pegemanyfar [41] performed Reynolds-averaged Navier–Stokes (RANS) simulations of an RQL combustor, observing that quenching occurred between 30 and 40% of the total combustor length. However, the study also identified hot spots resulting from near stoichiometric combustion significantly further downstream. This implies a relatively slow mixing process which, within the context of the current model, would be characterised by a larger τ_{dil}, leading to elevated NO_x emissions.

The primary zone residence time $\tau_{primary}$ describes the duration until cooling air is added. Pegemanyfar [41] provides residence time distributions at the primary zone exit plane with a mean value of approximately 3 to 4 ms. For the GT-309, Heywood and Mikus [37] describe a decreasing mean primary zone residence time from 11.2 to 6.8 ms for 50 and 100% load, respectively.

Model calibration and validation with an in-service combustor requires some description of key parameters. For the combustor of the V2500 turbofan engine sufficient literature statements were found. The model setup for the V2533-A5 is summarised in Table 2. All other inputs result from cycle calculation. With most model parameters originating from literature statements, two parameters were adjusted to calibrate to emission measurements. The dilution timescale parameter c_{dil} was used as the main calibration parameter resulting in the overall scale of NO_x predictions. The primary zone length parameter $c_{primary}$ was calibrated for the 30% thrust point, as it is near stoichiometric in the primary zone.

Figure 6a shows the sea-level static (SLS) NO_x emissions at 100, 85, 30 and 7 % of rated thrust (landing and take-off operations (LTO)) of the V2533-A5 engine (strongest variant of the V2500 engine family). Measurements, reported in the International Civil Aviation Organization (ICAO) emissions databank [42], are plotted alongside. The model is able to accurately reproduce the engine emissions across the different thrust levels, with some deviation at the lowest thrust setting.

https://doi.org/10.1017/aer.2026.10240 Published online by Cambridge University Press

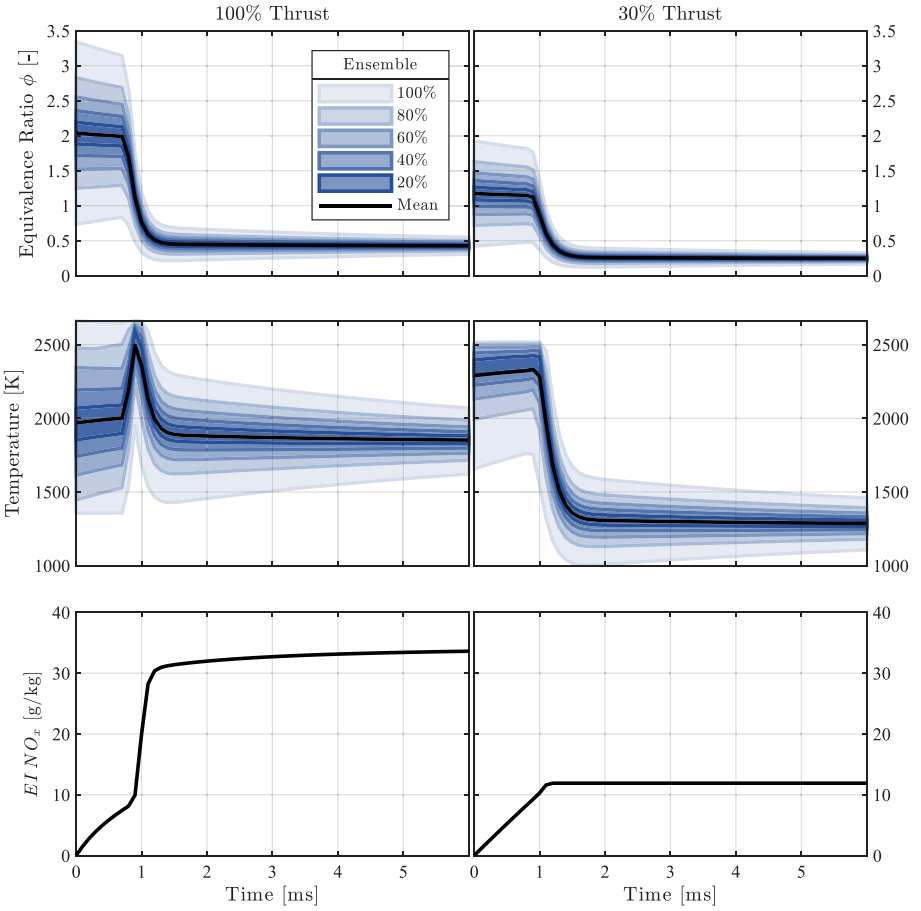


Figure 7. NO_x *model evolutions including stochastic ranges for the V2533-A5 at full and* 30 *% thrust.*

For the combustor analysed here, the dilution timescale resulting from c_{dil} is most sensitive on NO_x emissions. To accurately replicate the V2533-A5 NO_x measurements, a relatively short primary zone and very quick quenching was required. The evolutions of the equivalence ratio, temperature and the resulting NO_x is given in Figure 7 for full and 30 % thrust. At full thrust the primary zone shows the described $\bar{\phi} = 2$ with a wide distribution due to initial unmixedness. The temperatures and NO formation peaks during the stoichiometric crossing in the quenching phase. The 30 % thrust point shows a near stoichiometric primary zone, resulting in quenching quickly stopping NO formation.

Comparison with the findings of Pegemanyfar [41] reveals some important differences. Specifically, at full thrust, the temperature peak due to stoichiometric crossing occurs around 1 ms after the initial combustion in the primary zone, a transition much more rapid than reported by Pegemanyfar [41]. This discrepancy may stem from inherent differences in combustor geometry or signify specific model limitations. While the local equivalence ratio is modelled stochastically, the dilution is not. The rich jet does not uniformly experience quenching. However, since this non-uniformity is expected to exert a linear influence on NO_x formation, the current model presents a simplified yet accurate approach, as the calibration of c_{dil} compensates the simplified physics.

Figure 8 shows the model parameter sensitivities. The highest sensitivity is seen with the parameters describing the initial state in the combustor: β and s_0. With these factors fixed by the combustor technology, the main drivers are the dilution and primary zone length timescales c_{dil} and $c_{primary}$ depending on the thrust case. As the 30% thrust case has a near-stoichiometric primary zone, it is most affected by

https://doi.org/10.1017/aer.2026.10240 Published online by Cambridge University Press

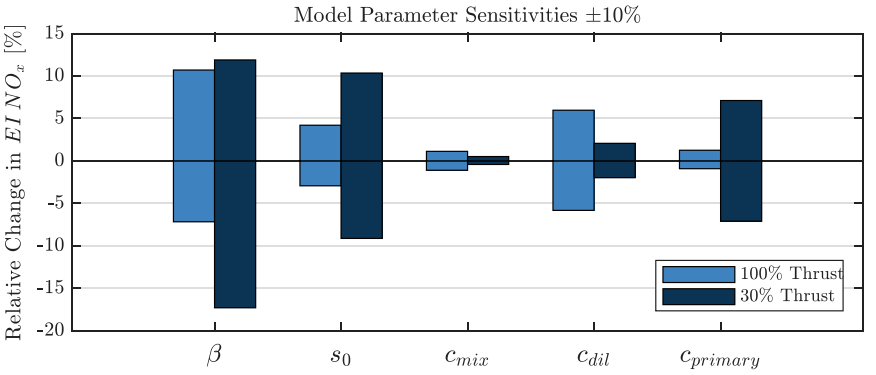


Figure 8. *Joule combustor* NO_x *model parameter sensitivity for the V2533-A5 at full and* 30 *% thrust.*

a variation of the primary zone setup. Under these rapid-quenching conditions, the homogenisation rate (τ_{mix}) becomes a secondary driver for NO_x production. With the relatively slow rate ($c_{mix} = 5$) there is still considerable variation in the local temperature towards the combustor exit plane.

2.3.4. Setup for near-future combustor

Due to limited data availability, the presented model was initially calibrated to the V2533-A5 engine. To account for the future entry-into-service of the investigated engine architecture, the model was subsequently adjusted to represent a future low-NO_x combustor. This was achieved by first calibrating an empirical NO_x correlation to the V2533-A5 engine and then applying a literature-based technology factor representative of a near-future combustor. The combustion-zone timescale parameters were subsequently adjusted until the physics-based model reproduced the NO_x formation implied by this technology factor.

A widely used empirical correlation for the estimation of aero-engine NO_x is described in the gas turbine simulation environment GasTurb [43], that is referenced here as the T_3-p_3 method:

$$s_{NO_x} = \left(\frac{p_3}{2965\,kPa}\right)^{0.4} \cdot exp\left(\frac{T3 - 836\,K}{194\,K} + \frac{6.29 - 100 \cdot WAR_{amb}}{53.2}\right) \tag{20}$$

This correlation requires the combustor inlet temperature T_3, pressure p_3 and optionally the ambient humidity WAR_{amb}. The emission index can be estimated by multiplying the severity factor s_{NO_x} with a technology factor c_s:

$$EI\,NO_x = c_s \cdot s_{NO_x} \tag{21}$$

Kurzke [43] provides $c_s = 32$ for conventional combustors and $c_s = 23$ for dual annular combustors. For the V2533-A5 engine, calibration against the ICAO databank SLS-LTO NOx emissions yielded $c_s = 18$, which provided good agreement with the reported data (Figure 6a). The increased emissions around 30% thrust due to a stoichiometric primary zone are not captured by this simple empirical correlation. For near-future projected lean direct injection combustors, $c_s = 12.4$ was calculated [44]. The authors state that 70% of the inlet air flows through the injectors, which would enable a model setup using $\beta = 0.7$. However, for the CCE the use of a lean direct injection combustor is questionable, due to the high level of inlet vitiation and the low heat addition in the combustor during typical cruise operation. To ensure consistent flammability a rich primary zone is likely required. To account for reduced NO_x emissions of a near-future combustor the model was calibrated to $c_s = 12.4$ (Figure 6b) by only reducing the dilution and primary zone timescale parameters ($c_{dil} = 0.17$, $c_{primary} = 0.19$). It is noted, that this level of quick quenching may be unrealistically fast, and it is recommended to study the model adaptation to future combustors in more detail.

https://doi.org/10.1017/aer.2026.10240 Published online by Cambridge University Press

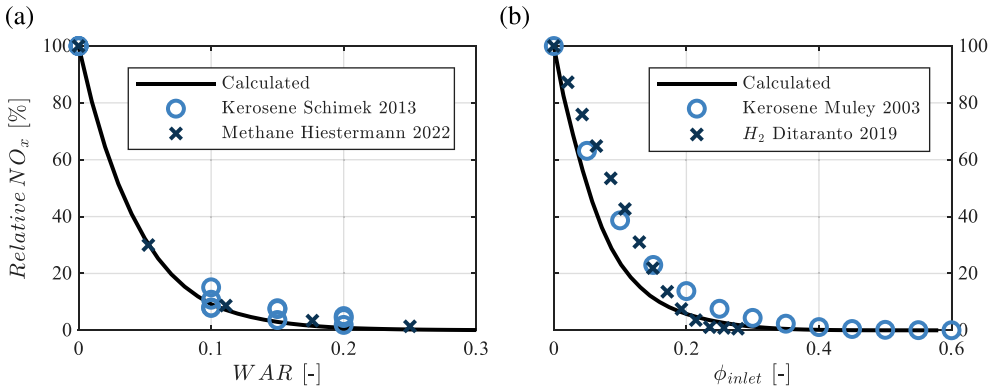


Figure 9. *Relative* NO_x *reduction with (a) WAR and (b) precombusted air.*

2.3.5. Effect of vitiated inlet air

Similar to the piston engine, the effect of humidified air on NO_x emissions is twofold: it involves the linear reduction of adiabatic flame temperature with increasing water content and a direct chemical impact on reaction kinetics through the suppression of key radical species, such as atomic oxygen. Schimek et al. [45] experimentally demonstrated that the chemical influence is stronger than the purely thermal effect, by comparing it to a nitrogen dilution stream with identical adiabatic flame temperature. Conversely, Hiestermann et al. [46] attributed most of the NO_x reduction to the reduction in maximum temperature, in a numerical study of methane combustion. In ultra-wet environments (up to 50% steam), Göke and Paschereit [47] demonstrated that NO_x reduction is driven by the chemical suppression of the thermal, N_2O and NNH pathways via radical scavenging. However, they noted that steam injection can simultaneously increase prompt NO_x in natural gas flames due to elevated CH radical concentrations.

The present study considers only premixed water vapor (e.g. originating from the piston engine), rather than direct water injection into the gas turbine, which would likely offer a higher NO_x reduction potential. The predicted NO_x reduction as a function of the water–air ratio $WAR = \dot{m}_{water}/\dot{m}_{air}$ is presented in Figure 9a, showing strong correlation with literature data. [45] analysed the effect of steam dilution at different equivalence ratios and nozzles, leading to multiple data points for the same *WAR*. The prediction will slightly vary depending on baseline NO_x, due to the exponential nature of thermal NO formation. The relatively high initial NO_x of the V2533-A5 at full thrust therefore shows a very steep decrease.

The use of precombusted inlet air represents a potent strategy for mitigating NO_x emissions through various architectural implementations. In EGR systems, a fraction of the exhaust gas is recirculated to the inlet; similarly, in staged combustion, sequential combustors, such as inter-turbine burners, utilise vitiated streams. Comparable conditions are found in the CCE, where the exhaust gases of the piston engine are funnelled into the downstream combustor, leading to a significant amount of inlet air vitiation depending on system operation. The underlying physical mechanisms mirror those of water injection: a reduction in adiabatic flame temperature and a lowering of the inlet oxygen concentration.

The relative reduction in NO_x emissions resulting from precombusted inlet air is depicted in Figure 9b. To simplify, similar to Muley and Lear [8], it has been assumed that the inlet temperature remains constant (e.g. via a recirculation cooler), with adjustments made only to the inlet mass flow, the inlet FAR and the exit FAR. Compared to the study performed by Muley and Lear [8], the current model predicts a more significant reduction in NO_x. This discrepancy is likely attributable to the differing modelling approaches. While Muley and Lear [8] use a single-zone PSR at stoichiometric conditions, the stochastic model used in this study captures the local temperature peaks and their sensitivity to oxygen depletion, possibly thereby predicting a higher relative reduction in thermal NO formation. The Joule combustor in the CCE will see high inlet equivalence ratios, where the model aligns reasonably well with the literature reportings.

https://doi.org/10.1017/aer.2026.10240 Published online by Cambridge University Press

Table 3. *Preliminary parameters for the LR FDP-CCE at Mid-cruise*

Parameter	Piston engine
λ [−]	2
v_{mean} $[m/s]$	15
Bore $[m]$	0.23
Bore-stroke ratio [−]	1
SOC $[deg]$	350
EOC $[deg]$	$SOC + 50$
Compression ratio [−]	7.31
T_{in} $[K]$	710
p_{in} $[Pa]$	$9.87e5$
p_{peak} $[Pa]$	$150e5$
Piston cylinder number [−]	20
λ_0 [−]	1
c_A [−]	0.9
Parameter	**Joule combustor**
Fuel flow $[kg/s]$	0.2144
Inlet mass flow $[kg/s]$	40.73
Inlet vitiation FAR_{in}	0.0143
T_{in} $[K]$	1029
p_{in} $[Pa]$	$9.17e5$
β [−]	0.22
s_0 [−]	0.3
c_{mix} [−]	5
c_{dil} [−]	0.17
$c_{primary}$ [−]	0.19

The stochastic model shows solid capability in capturing the NO_x formation in gas turbine combustors. While relying on five model parameters, most of these can be well defined from a general description of the combustor. The model is also capable of capturing the effects of vitiated air on NO_x emissions. For the purpose of emission estimation in the CCE, this model is deemed effective.

3.0 Results and discussion

To assess the capability of the NO_x models to estimate CCE emissions, component-level studies are performed. These focus on the initial piston emissions and their mitigation via water injection and EGR. Then a first assessment of the combustor and overall NO_x emissions is performed, including a first look into the NO reburning potential.

3.1. FDP-CCE setup

To this end, a reference point at mid-cruise for the long-range (LR) sustainable aviation fuel (SAF)-fueled aircraft is defined, resulting from a propulsion system calculation. The FDP-CCE setup and system-level calculation are described in detail by Lin et al. [22]. Table 3 lists the reference point setup used in the following studies. Unless indicated, these parameters are kept constant.

The combustor setup keeps the setup from the V2533-A5, with the dilution and primary zone timescale parameters modified for a near-future combustor, as described above. In this preliminary design phase, the absolute dimensions of the combustor have yet to be established. Baseline dimensions

https://doi.org/10.1017/aer.2026.10240 Published online by Cambridge University Press

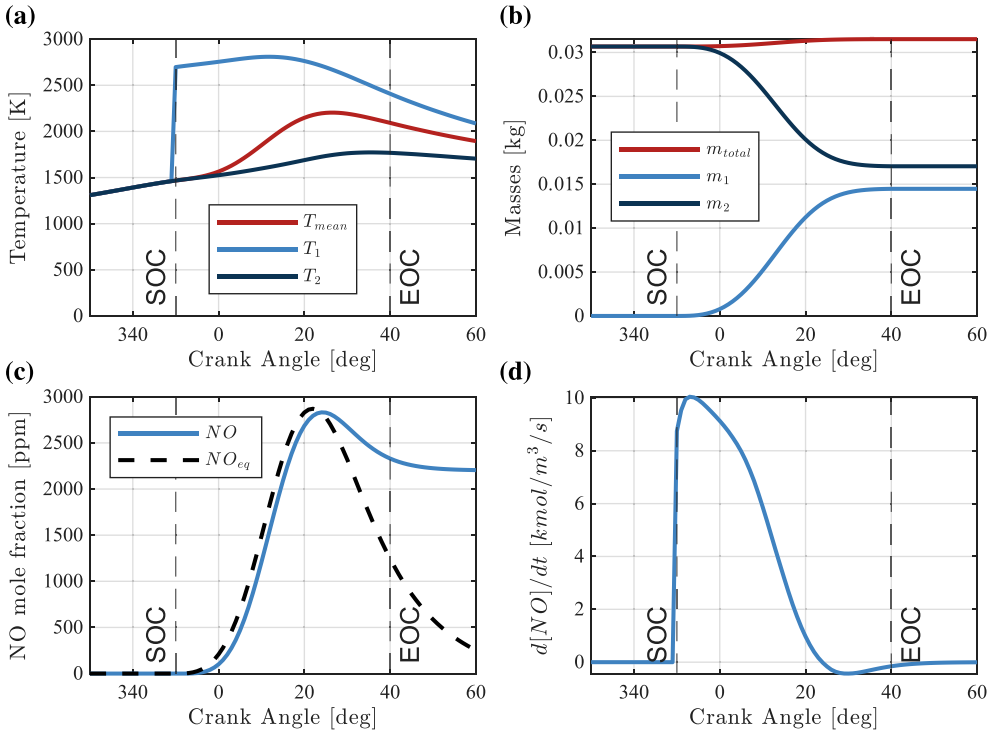


Figure 10. *FDP-CCE piston* NO *formation at reference point (see Table 3).*

for the combustor were established by scaling the V2500 combustor design. The cross-sectional area was adjusted based on the core size ratio, with the injector nozzle diameter calculated using square-root scaling of that same ratio.

3.2. Piston emissions

An initial assessment of the FDP NO_x emissions is conducted at component level. The analysis is performed under fixed, constant-geometry (off-design) conditions, which inherently leads to variations in both produced power and exhaust energy. Although system-level sizing effects and their implications are not addressed at this stage, these preliminary calculations provide valuable insight into the underlying emission formation behaviour. The general trends identified here are therefore expected to remain valid and informative when extended to future, fully sized system studies.

The NO formation of the reference point is visualised in Figure 10. The temperature of the combusted zone T_1 is significantly higher than the mean temperature, with both converging only much later than *EOC* in the expansion stroke after NO freeze. At this reference point with $\lambda = 2$, only a portion of the uncombusted zone is transferred to the combusted zone. The evolution of the NO molar fraction shows close alignment with the theoretical steady-state equilibrium fraction until NO freeze, due to dropping temperatures in the expansion stroke. This and the reduction after peak NO highlight the equilibrium limitation.

Figure 11a shows the NO_x emissions with varying air-excess ratio λ. Generally, NO_x decreases with λ as the mass in the combusted zone decreases, while its temperature is only minimally affected. The difference between single zone mean and combusted-zone temperature (Figure 11c) highlights the importance of resolving the high-temperature regions. Only under stoichiometric conditions does the single zone mean cylinder temperature lead to NO_x formation predictions similar to those obtained using the resolved

https://doi.org/10.1017/aer.2026.10240 Published online by Cambridge University Press

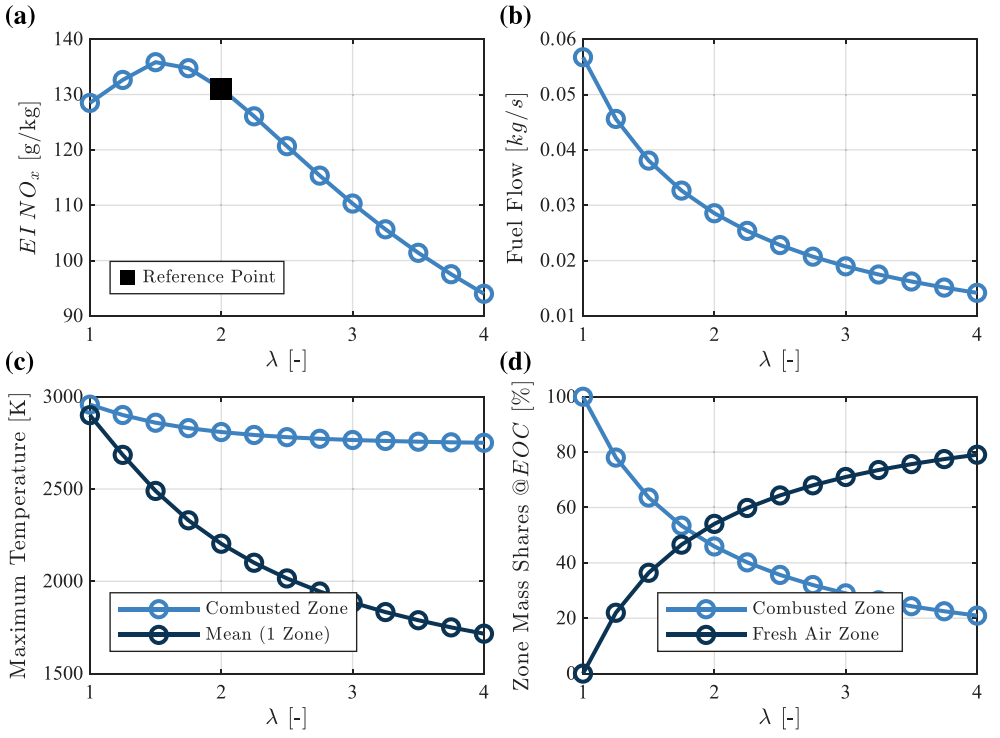


Figure 11. *FDP-CCE piston global air-excess ratio λ study.*

combusted-zone temperature. At $\lambda < 1.5$ a reduction can be observed. While the NO_x mass is decreasing nearly linearly with λ, the fuel flow is seeing an exponential decrease, leading to an initial peak in the emission index at $\lambda \approx 1.5$.

3.3. Piston NO_x *mitigation via vitiated air*

With the significant NO_x formation in the piston engine, appropriate mitigation might be required. In the following water injection and EGR are assessed.

Water addition in the piston can take place at various locations. Here two limiting cases are considered: premixed and directly injected proportional to the fuel combustion rate. Premixed water addition is representative of intake-charge humidification concepts such as the humid air motor [48], where water vapour is introduced upstream of the cylinder and is assumed to be homogeneously distributed throughout the charge. Such concepts reduce NO_x formation mainly by increasing the heat capacity of the working fluid, reducing oxygen availability and lowering peak combustion temperatures. Figure 12 compares the two water addition cases over a range of *WFR*s. The NO_x reduction potential of premixed water is lower than with direct injection. In the model for direct injection all injected water is assumed to remain in the combusted, NO_x producing zone, while premixed water results in a homogeneous distribution with a lower *WAR* in the combusted zone (see Figure 12b). Furthermore, premixed water is heated during compression and is therefore already at the start-of-combustion (SOC) temperature, whereas directly injected water enters at the prescribed injection temperature. The effective cooling potential in the NOx-forming region is therefore lower for premixed water addition. This implementation of direct water injection could be seen as the optimal injection case, with an impressive mitigation potential. For the water-fuel emulsion study shown in Figure 3 the model indicated the correct relative NO_x decrease at higher *WFR*, signifying that such reductions are achievable in real engines. The injection through dedicated water injection nozzles allows for more design flexibility.

https://doi.org/10.1017/aer.2026.10240 Published online by Cambridge University Press

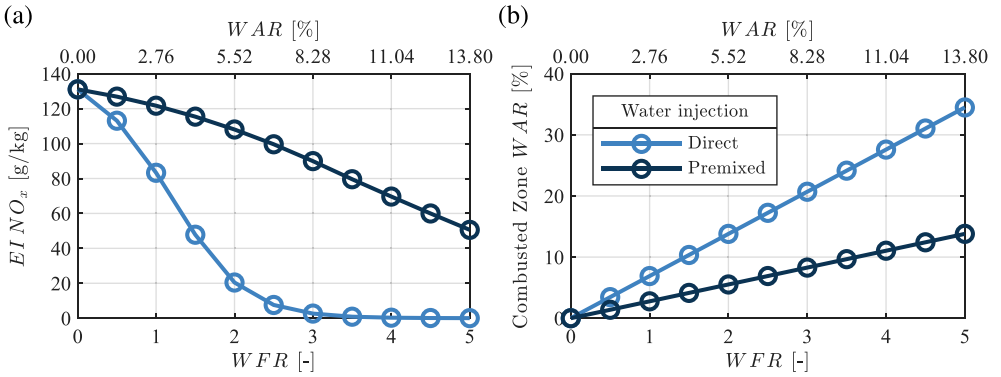


Figure 12. *Water injection premixed versus direct injection ($T_{inj} = T_{inlet} = 710\,K$).*

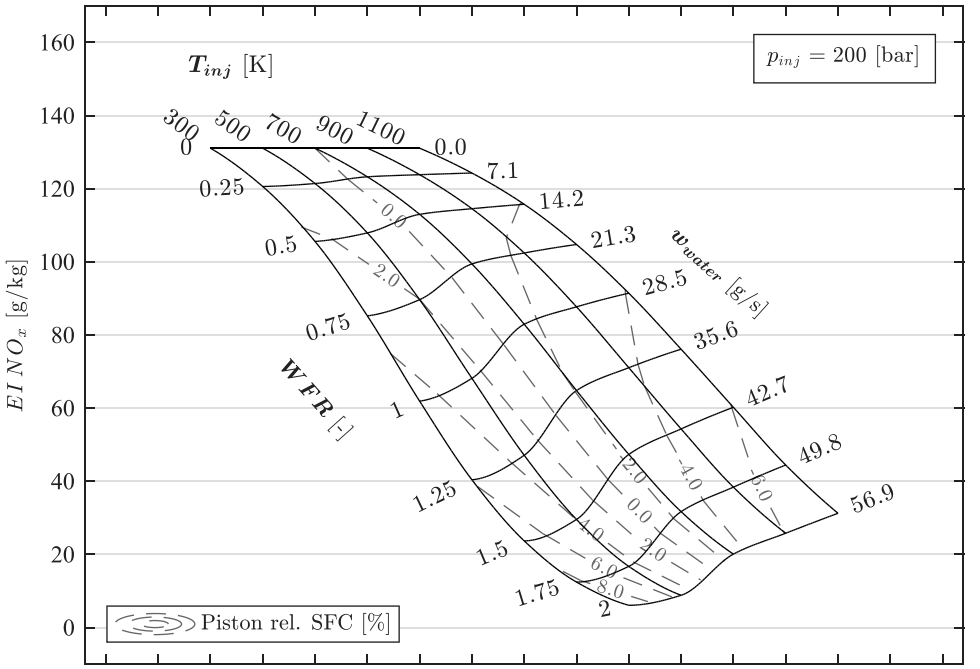


Figure 13. *Direct water injection in the FDP at different WFRs and water injection temperatures T_{inj} for given piston geometry. The required water provision w_{water} is per cylinder.*

Figure 13 illustrates the NO_x reduction potential achieved through direct water injection across varying injection temperatures T_{inj}. Considerable reductions in NO_x emissions are achieved. Direct water injection at ambient temperatures (no vaporisation or recuperation) and $WFR = 1$ results in a significant NO_x reduction of 56%. Per cylinder this requires a water mass flow of 28.5 g/s. For the above-mentioned engine setup with 10 FDP units, each with 2 cylinders, this results in a water requirement of 570 g/s per engine.

Figure 13 also includes isolines for the relative change in *SFC* with respect to the dry reference case in Table 3. Since the FDP subsystem acts purely as a gas generator in the investigated architecture, the *SFC* trends should not be interpreted as a precise indicator of overall propulsion-system performance. In particular, the system-level impact of water injection also depends on the downstream turbine, pressure

https://doi.org/10.1017/aer.2026.10240 Published online by Cambridge University Press

losses, water preparation and heat-rejection or recuperation effects, which are not resolved in the present component-level analysis. *SFC* improves with T_{inj} as expected. The effect of direct water injection temperature on *SFC* is governed by two competing contributions: external enthalpy addition through the injected water and the in-cylinder enthalpy required to heat the injected water to the cylinder-gas temperature. In the phase-change region (between 600 and 700 K), both effects approximately balance for the investigated engine setup.

For the analysed operating point, a water injection pressure of 200 bar was assumed, with a margin to the considered peak cylinder pressure of the considered piston condition (see Table 3). Across the full operating envelope, however, the required injection pressure would have to be adapted to the instantaneous cylinder pressure. In particular, for operating points approaching the maximum cylinder pressure reported by [22], injection pressures above 200 bar would be required. At this pressure, the saturation temperature of water is approximately 637 K. As observed in the figure, liquid water injection yields greater NO_x reduction compared to steam injection, which is attributed to the substantial reduction in peak cylinder temperature driven by the latent heat of vaporisation. While liquid injection is more effective for NO_x mitigation and allows for simpler liquid handling, the associated vaporisation can introduce risks, such as delayed initial combustion and potential flame quenching. An additional operating regime exists for injection pressures above the critical pressure of water, $p > p_{crit}$. If the injection temperature remains below the critical temperature, $T < T_{crit}$, the water is a compressed, liquid-like fluid rather than steam. Upon heating, it may pass through the pseudo-critical region, where large variations in thermophysical properties and elevated heat capacity can provide strong cooling without a classical two-phase transition. This regime could therefore combine liquid-like handling with some of the thermal benefits associated with pseudo-boiling. Fully supercritical injection, with both $p > p_{crit}$ and $T > T_{crit}$, could also be advantageous because its single-phase nature promotes efficient heat transfer within the recuperation system and avoids the complexities of two-phase flow [49].

Implementing piston water injection in the FDP-CCE architecture presents specific thermal integration opportunities. While exhaust gas heat recovery may enhance overall efficiency, the lower temperature gradient necessitates bulky heat exchangers. Alternatively, the piston system offers a distinct heat source, as the piston engine requires significant heat rejection. Recuperating heat from the piston system could improve thermal efficiency while enabling a more compact design. However, given the complexity of the CCE architecture, any such recuperation system must be designed as fail-safe; a malfunction in the water injection or heating system must not compromise the continuous operation of the piston engine.

The critical issue for the applicability of water injection in any aero-propulsion system is the water source. The simplest potential water provision source would be a water tank, which would add significant mass. For greater reduction of cruise NO_x emissions hybridisation with a fuel cell system can be considered, with the fuel cell product water harvested for combustion vitiation [50]. Seitz [51] gives a compact overview over the NO_x reduction potential in a conventional turbofan at different levels of hybridisation. This stretches from a fuel cell system for all-electric aircraft subsystems, active aerodynamics, cycle-integrated hybrid, fuselage boundary layer ingestion fan to single gas turbine propulsion. For a given water mass flow, the reduction potential is even higher for the piston application, due to the much higher initial emissions, effective targeting of hot spots by direct injection and the increased specific work output of a CCE cycle. Alternatively, water could be condensed out of the CCE exhaust stream, similar to the water-enhanced turbofan [52]. Such a setup would require extensive heat exchangers for exhaust gas cooling and condensation.

A similar NO_x reduction potential can be found with EGR. The intake mixture consists of fresh air and recirculated exhaust gas. The EGR rate is defined as the mass fraction of the total exhaust gas that is recirculated:

$$EGR = \frac{\dot{m}_{EGR}}{\dot{m}_{exh}} \tag{22}$$

https://doi.org/10.1017/aer.2026.10240 Published online by Cambridge University Press

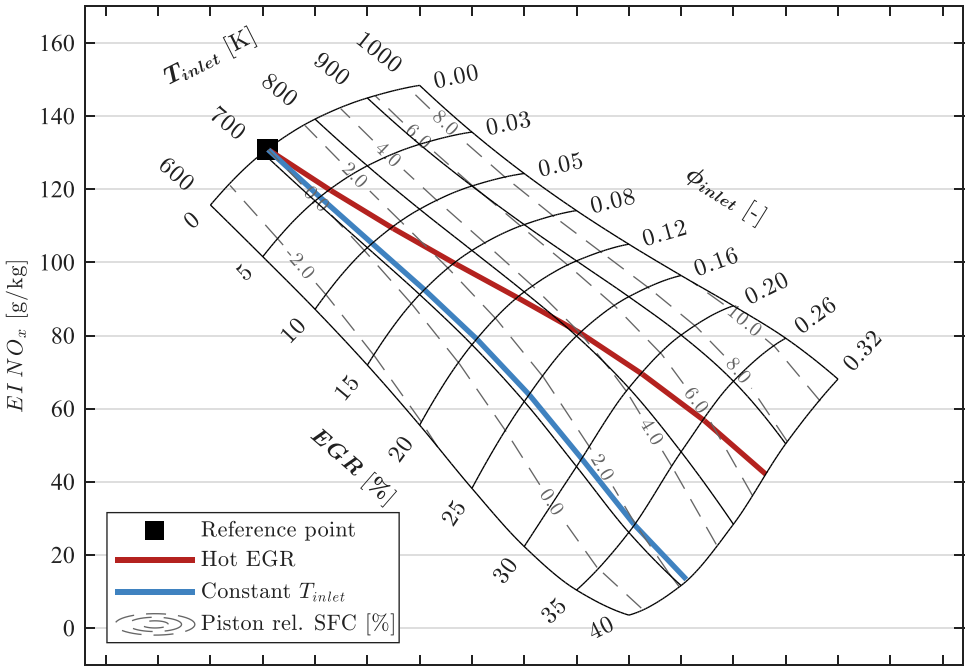


Figure 14. *Direct recirculation of the FDP engine exhaust at different inlet temperatures for given piston geometry.*

Assuming the recirculated gas maintains the chemical proportions of the exhaust (e.g. no scrubbing), the FAR of the intake mixture can be expressed as a function of the exhaust FAR_{exh} and the EGR rate:

$$FAR_{in} = FAR_{exh} - \Delta FAR = \frac{EGR \cdot FAR_{exh}}{1 + FAR_{exh} \cdot (1 - EGR)} \tag{23}$$

For the EGR and inlet temperature study, shown in Figure 14, a constant combustion delta is maintained between the inlet and exhaust $\Delta FAR/FAR_{stoich} = \phi_{exh} - \phi_{inlet} = 0.5$. Figure 14 shows the reduction potential with the recirculation rate EGR and piston inlet temperature T_{inlet}. The decrease in NO_x for lower T_{inlet} at $EGR = 0$ highlights the potential for intercooling.

NO_x emissions decline near-linearly with the EGR rate, with the rate of reduction even increasing slightly at higher EGR percentages. This slightly weaker curvature is believed to be related to the mixture approaching the range where the NO_x trend in Figure 11 decreases toward stoichiometric conditions. The impact of EGR on performance and emissions depends on thermal management. In the hot EGR case, where exhaust gases are recirculated without heat rejection, the resulting increase in intake temperature leads to a more moderate reduction in NO_x and a penalty in SFC due to reduced volumetric efficiency. On the other hand, by utilising heat exchangers to achieve cool EGR, the intake temperature remains neutral. Overall, the model predicts significant NO_x reduction potential across the selected conditions. By recirculating 30 % of exhaust gases, NO_x emissions are reduced by 65 and 47% for the cool and hot EGR configurations, respectively.

In the FDP-CCE EGR could be achieved in different ways. The simplest but least-effective approach is internal EGR or poor scavenging. As with hot EGR the NO_x reduction is significant while not as effective as at lower temperatures. However, this comes at a penalty of both worse thermal efficiency and specific power. A rerouting of FDP engine exhaust to the piston engine inlet allows the intermediate installation of a heat exchanger. Lastly, on propulsion system level, a recirculation from a bleed port in the turbine section to before the FDP system might be possible. The exhaust gases now also contain the combustor exhaust and are diluted by numerous cooling streams. This will require recompression, since

https://doi.org/10.1017/aer.2026.10240 Published online by Cambridge University Press

Table 4. *LR FDP-CCE* NO_x *emissions at mid-cruise without mitigation*

		EI NO_x $[g/kg]$		
$\frac{w_{f,piston}}{w_{f,total}}$ $[-]$	λ $[-]$	Piston	Combustor	Overall
0.64	2.33	124	1.51	77
0.73	2.09	131	1.55	97
0.80	1.90	132	1.62	103

the EGR stream must be brought to the pressure level required at the reinjection location upstream of, or within, the FDP compression process. In addition, pressure matching between the turbine bleed location and the EGR reinjection point represents an important design constraint. This may become particularly challenging during part-load operation, where variations in the pressure ratio of the FDP system can lead to a mismatch between the available bleed pressure and the required reinjection pressure. However, this arrangement might offer advantages in its geometric integration. One concept for an intercooled FDP-CCE sees the intercooler installed behind the piston system, next to the turbine section. The recirculation ahead of the intercooler would thereby require minimal additional ducting and the intercooler can be extended to also reject EGR gas heat. This would also result in an increased heat capacity for both the turbine section and the piston compressor. The FDP heat management typically considers bypass air as heat sink. This could also be used for recirculation cooling, either as a separate cooler or via integration with an intercooler.

Despite these promising options, EGR may introduce challenges for engine operation. Fouling consists of soot and unburned hydrocarbons depositing on EGR surfaces, particularly in heat exchangers. Dry EGR is considered impractical for aeronautical applications due to the significant weight penalty of the required hardware, such as scrubbers or moisture separators. Furthermore, drying the recirculated gas offers no advantage for NO_x reduction; in fact, the high specific heat capacity of water vapour in wet EGR provides superior thermal suppression of the flame temperature compared to dry exhaust. However, it is noted that the omission of a drying stage introduces severe technical challenges, particularly the risk of engine corrosion and the potential for acid formation from condensed combustion products in the intake manifold. The sulphuric acid considerations are relevant for sulphur containing fuel [32]. It can be assumed that SAF is practically sulphur-free, while H_2 is completely sulphur-free.

3.4. Joule combustor emissions

The piston engine exhaust, including NO_x emissions, are input into the combustor model for an initial assessment of the engine-out emissions. An initial overview is given in Table 4 for three different piston fuel share cases. As shifting fuel burn from the piston engine to the combustor decreases the system efficiency, the overall design changes. The three points shown here result from system level calculations, that result in a change of piston parameters. While the piston NO_x emissions change due to a varying air-excess ratio, the combustor emissions change little due to high level of inlet vitiation. As more fuel is shifted towards the piston engine the overall *EI* NO_x increases. These overall NO_x emissions are about $5-8$ times more than that of a similar advanced turbofan combustor, clearly highlighting the necessity for significant NO_x mitigation measures. This range also aligns with the findings of Kaiser [17].

3.4.1. NO reburn potential

As previously mentioned, the high inlet emissions in the Joule combustor present the potential for NO reburning. While Glarborg et al. [13] also demonstrated a substantial reburn potential in H_2 combustion, most research focused on the reduction driven by the local availability of hydrocarbon radicals (CH_i). Myerson [53] established that specific oxygen-to-fuel ratios are required to initiate the necessary radical

https://doi.org/10.1017/aer.2026.10240 Published online by Cambridge University Press

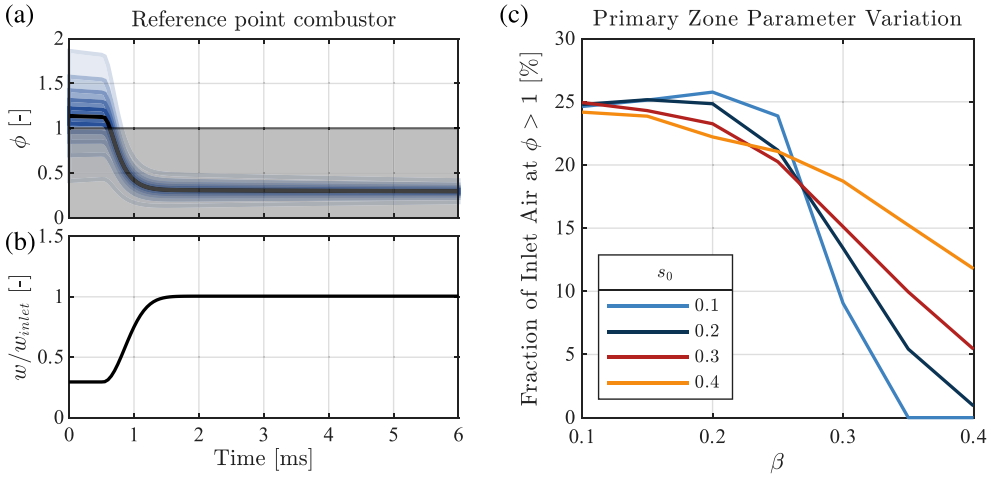


Figure 15. *Assessment of* NO *reburn potential conditions in the Joule combustor.*

pool, but excess oxygen rapidly destroys these species. Consequently, reburn potential is maximised in zones maintained at locally rich equivalence ratios, even if global conditions are fuel-lean.

This local richness is preserved by imperfect mixing. Nicolle and Gagaut [54] demonstrated that increased unmixedness delays auto-ignition, widening the temporal window where peak radical concentrations overlap with inlet NO. This is supported by Ditaranto et al. [12] and Sullivan-Lewis et al. [55], that confirmed that conditions favouring longer residence times at small scales, such as diffusion, stabilisation or reduced swirl intensity, enhance radical survival. Furthermore, high water concentrations in the vitiated stream were found to improve efficiency by chemically quenching hydrocarbon oxidation, thereby preserving the reductant pool. Finally, while temperatures must be sufficiently high to overcome activation barriers, excessive heat combined with oxygen accelerates reductant destruction.

While the calculation of the NO_x reduction potential requires detailed chemistry, which is out of scope of the present study, the fundamental possibility of reburning with hydrocarbon radicals is estimated, by determining the fraction of the vitiated, high NO_x inlet flow that sees rich zones in the combustor.

Figure 15a and b shows the evolution of the equivalence ratio ϕ and the inlet mass flow fraction in the combustor. Despite the overall lean conditions and the low amount of fuel injection in the Joule combustor, the primary zone is majorly rich at higher temperatures, signifying conditions which may be favourable for NO reburning. While here the primary zone timescale $\tau_{primary}$ was kept unchanged, it would be possible to extend this as to give sufficient time for the back reactions, if need be. In Figure 15c the primary zone parameters β (fraction of inlet flow in primary zone) and s_0 (initial unmixedness) are varied resulting in a changing fraction of the inlet flow seeing rich conditions. As β is increased the equivalence ratio ϕ decreases, decreasing the amount of rich zones. The unmixedness s_0 has a different effect depending on whether the mean primary zone equivalence ratio is rich or near stoichiometric. At the analysed operating point, up to 26% of the vitiated inlet air are going through rich zones. This fraction will increase as fuel is shifted from the piston engine to the Joule combustor. Together with the high inlet NO_x this signifies that NO reburning can potentially decrease overall CCE emissions. But this initial hypothesis would have to be confirmed through in-depth numerical analysis and experimental validation.

3.5. Model assessment and further work

3.5.1. Piston model: evaluation and refinement

The piston model effectively captures general NO_x trends in the studied piston engines using only a single calibration parameter. While physical influences such as in-cylinder turbulence, which dictates

https://doi.org/10.1017/aer.2026.10240 Published online by Cambridge University Press

quenching, are currently absent, this omission is deemed acceptable given the early development stage of the FDP and the associated lack of setup data. Future development should prioritise higher-fidelity numerical or preferably experimental tests as a baseline for the NO_x model. This would facilitate increased model complexity, such as the implementation of a parallel mixing mass flow within the two-zone framework or a transition to a multi-zone model. The single air-excess ratio is capable of describing the general NO_x trends for direct/late injection. On the contrary, in early injection or premixed combustion, the local variation of equivalence ratio is not captured by the model.

3.5.2. Combustor model: evaluation and refinement

The stochastic combustor model demonstrates a high capability for capturing NO_x formation trends in gas turbines. It was found that in RQL architectures, next to the primary zone setup, the dilution or quenching timescale is the primary driver of NO_x prediction accuracy, marking it as a critical area for future refinement. Furthermore, while the current model uses a standard normal distribution, future work could explore the implementation of non-normal PDFs should empirical data support such a shift. Finally, extending this stochastic framework to other combustor architectures, such as lean-premixed, micro-mix, staged or recursive combustion, would be a valuable next step in validating the model's versatility. The assessment of the reburning potential requires the integration of a more complex kinetics scheme, including at minimum the prompt NO path.

3.5.3. System-level NO_x *estimation, mitigation & engine design*

The FDP-CCE engine-out NO_x emissions are dominated by the high piston engine NO_x formation. These initial results highlight the issue at hand, but it is important to highlight that these are component level findings without any optimisation. The next step in the research is the integration of the described NO_x models into the propulsion system performance synthesis framework. This will then allow for full system optimisation to find a balance between fuel burn improvement and NO_x emissions, including more advanced architectures utilising intercooling, water injection or EGR. The latter two mitigation options were found to offer a high NO_x reduction potential.

4.0 Conclusion

This work described two models for the estimation of NO_x emissions in piston engines and gas turbine combustors. Generally, they showed good predictive capability for capturing the main NO_x trends for different loads, water injection and EGR. The piston NO_x emissions at a representative mid-cruise point were found high at $EI\,NO_x = 131$ g/kg. The downstream combustor produced little additional NO_x due to the vitiated inlet air, resulting in engine-out emissions of 97 g/kg. NO reburning might reduce these emissions, as for this initial point up to 26% of piston exhaust gas sees rich conditions in the combustor. Both water injection and EGR proved highly effective for NO_x abatement. Specifically, a 60% reduction could be achieved with a $WFR = 1.1$ or cooled recirculation of 28% of the piston exhaust gases. Building on this initial component-level assessment, a system-level optimisation can now be performed to minimise the overall climate impact of the FDP-CCE concept.

Financial support. The studies were conducted in the project MINIMAL (Minimum environmental impact ultra-efficient cores for aircraft propulsion). MINIMAL has received funding from the European Union under the Horizon Europe grant agreement No. 101056863 and from the UK Research and Innovation (UKRI) under contract No.10040930, 10053292 and 10039071. Views and opinions expressed are, however, those of the authors only and do not necessarily reflect those of the European Climate, Infrastructure and Environment Executive Agency (CINEA). Neither the European Union nor CINEA can be held responsible for them.

Competing interests. The authors declare no competing interests.

https://doi.org/10.1017/aer.2026.10240 Published online by Cambridge University Press

References

[1] Kaiser, S., Seitz, A., Donnerhack, S. and Lundbladh, A. Composite cycle engine concept with hectopressure ratio, *J. Propul. Power*, 2016, **32**, pp 1413–1421. https://doi.org/10.2514/1.b35976

[2] Nickl, M. and Kaiser, S. Evaluation of piston engine modes and configurations in composite cycle engine architectures, *CEAS Aeronaut. J.*, 2020, **11**, pp 391–400. https://doi.org/10.1007/s13272-019-00399-w

[3] Klingels, H. Wärmekraftmaschine mit Freikolbenverdichter. German Patent DE102012206123A1, 17 October 2013.

[4] Kaiser, S., Schmitz, K. and Klingels, H.E. Aero-engine concepts beyond 2030: part 2- the free-piston composite cycle engine, 2020. https://doi.org/10.1115/1.4048993

[5] Kaiser, S., Kellermann, H., Nickl, M. and Seitz, A., 'A composite cycle engine concept for year 2050', in *31st Congress of the International Council of the Aeronautical Sciences (ICAS 2018)*, Belo Horizonte, Brazil, 2018.

[6] Andreasen, A. and Nyggard, K.B. Water-in-fuel emulsion as marine engine fuel for reduced NOx and particulate emissions. Environmental Project No. 1380, Danish Environmental Protection Agency, 2011.

[7] Göke, S., Füri, M., Bourque, G., Bobusch, B., Göckeler, K., Krüger, O., Schimek, S., Terhaar, S. and Paschereit, C.O. Influence of steam dilution on the combustion of natural gas and hydrogen in premixed and rich-quench-lean combustors, *Fuel Process. Technol.*, 2013, **107**, pp 14–22. https://doi.org/10.1016/j.fuproc.2012.06.019

[8] Muley, N. and Lear, W. Effect of exhaust gas recirculation on thermal NOx formation rate in gas turbine engines, *41st Aerospace Sciences Meeting and Exhibit*, 2003. https://doi.org/10.2514/6.2003-503.

[9] Merker, G.P. and Teichmann, R. *Grundlagen Verbrennungsmotoren*, Springer Fachmedien Wiesbaden, 2019. https://doi.org/10.1007/978-3-658-23557-4

[10] Wang, Z. and Yang, X. NOx formation mechanism and emission prediction in turbulent combustion: a review, *Appl. Sci.*, 2024, **14**, p 6104. https://doi.org/10.3390/app14146104

[11] Chen, W., Smoot, L.D., Hill, S.C. and Fletcher, T.H. Global rate expression for nitric oxide reburning. Part 2, *Energ. Fuel*, 1996, **10**, pp 1046–1052. https://doi.org/10.1021/ef960007v

[12] Ditaranto, M., Hals, J. and Bjørge, T. Investigation on the in-flame NO reburning in turbine exhaust gas, *Proc. Combust. Inst.*, 2009, **32**, pp 2659–2666. https://doi.org/10.1016/j.proci.2008.07.002

[13] Glarborg, P., Kristensen, P.G., Dam-Johansen, K., Alzueta, M.U., Millera, A. and Bilbao, R. Nitric oxide reduction by non-hydrocarbon fuels. Implications for reburning with gasification gases, *Energ. Fuel*, 2000, **14**, pp 828–838. https://doi.org/10.1021/ef990186r

[14] Lamaris, V.T., Hountalas, D.T., Zannis, T.C. and Glaros, S.E. *Development and Validation of a Multi-Zone Combustion Model for Predicting Performance Characteristics and NOx Emissions in Large Scale Two-Stroke Diesel Engines. Volume 3: Combustion Science and Engineering*, 2009, pp 317–327. https://doi.org/10.1115/IMECE2009-11382

[15] Raptotasios, S.I., Sakellaridis, N.F., Papagiannakis, R.G. and Hountalas, D.T. Application of a multi-zone combustion model to investigate the NOx reduction potential of two-stroke marine diesel engines using EGR, *Appl. Energy*, 2015, **157**, pp 814–823. https://doi.org/10.1016/j.apenergy.2014.12.041

[16] Weisser, G.A. Modelling of combustion and nitric oxide formation for medium-speed DI diesel engines: a comparative evaluation of zero- and three-dimensional approaches (Doctoral dissertation). ETH Zurich, 2001. https://doi.org/10.3929/ethz-a-004317089

[17] Kaiser, S. Multidisciplinary design of aeronautical composite cycle engines. Doctoral dissertation, Technische Universität München, Munich, Germany, 2020.

[18] US EPA. How are Oxides of Nitrogen (NOx) defined in the NEI?, 2021. https://www.epa.gov/air-emissions-inventories/how-are-oxides-nitrogen-nox-defined-nei

[19] Wiebe, I. Semi-Empirical Expression for Combustion Rate in Engines, *Izvestiya Akademii Nauk SSSR, Otdelenie Tekhnicheskikh Nauk*, 1955, pp 286–289.

[20] Van Gerpen, J.H. Simulation of a combined-cycle engine. NASA Contractor Report NASA-CR-188232, Mechanical Engineering Department, Iowa State University, Ames, IA, USA, June 1991.

[21] Hohenberg, G.F. Advanced approaches for heat transfer calculations, SAE Technical Paper 790825; SAE International: Warrendale, PA, USA, 1979. https://doi.org/10.4271/790825

[22] Lin, Y.-H., Uhl, G., Winter, F., Lessis, A., Witzgall, F. and Seitz, A. Engine design study for free double piston integrated composite cycle engine, *Aerospace*, 2026. **13**, p 354. https://doi.org/10.3390/aerospace13040354

[23] Nickl, M., Winter, F. and Gümmer, V. Piston engine modelling for hydrogen fueled composite cycle engines, *IOP Conf. Ser., Mater. Sci. Eng*, 2022, **1226**, p 012033. https://doi.org/10.1088/1757-899X/1226/1/012033

[24] Winter, F., Lin, Y.-H., Nickl, M. and Seitz, A. Initial performance synthesis of a hydrogen-fueled free-double-piston composite cycle engine, 2024. https://doi.org/10.5281/zenodo.17485164

[25] Gerstle, M. Simulation des instationären Betriebsverhaltens hochaufgeladener Vier- und Zweitakt-Dieselmotoren, 1999. https://doi.org/10.15488/5614

[26] Li, R.C., Zhu, G.G. and Men, Y. A two-zone reaction-based combustion model for a spark-ignition engine, *Int. J. Engine Res.*, 2019, **22**, pp 109–124. https://doi.org/10.1177/1468087419841746

[27] Kozuch, P. Ein phänomenologisches Modell zur kombinierten Stickoxid und Rußberechnung bei direkteinspritzenden Dieselmotoren (Doctoral dissertation), 2004.

[28] Andersson, M., Johansson, B., Hultqvist, A. and Noehre, C. A predictive real-time NOx model for conventional and partially premixed diesel combustion, *SAE Technical Paper Series*, 2006. https://doi.org/10.4271/2006-01-3329

[29] Brückner, C., Pandurangi, S.S., Kyrtatos, P., Bolla, M., Wright, Y.M. and Boulouchos, K. NOx emissions in direct injection diesel engines– part 1: development of a phenomenological NOx model using experiments and three-dimensional computational fluid dynamics, *Int. J. Eng. Res.*, 2018, **19**, pp 308–328. https://doi.org/10.1177/1468087417704312

https://doi.org/10.1017/aer.2026.10240 Published online by Cambridge University Press

[30] Heider, G., Woschni, G. and Zeilinger, K. 2-Zonen Rechenmodell zur Vorausrechnung der NO-emission von Dieselmotoren, *MTZ- Motortechnische Zeitschrift*, 1998, **59**, pp 770–775. https://doi.org/10.1007/BF03226479
[31] Oppenauer, K.S. and Del Re, L. Hybrid 2-zone diesel combustion model for NO formation, *SAE Int. J. Engines*, 2010, **02**, pp 584–596. https://doi.org/10.4271/2009-24-0135
[32] Andreasen, A. and Mayer, S. Modelling of the oxidation of fuel sulfur in low speed two-stroke diesel engines. In *26th CIMAC World Congress on Combustion Engine Technology*, Bergen, Norway, 2010, Paper No. 39.
[33] Scappin, F., Stefansson, S.H., Haglind, F., Andreasen, A. and Larsen, U. Validation of a zero-dimensional model for prediction of NOx and engine performance for electronically controlled marine two-stroke diesel engines, *Appl. Therm. Eng.*, 2012, **37**, pp 344–352. https://doi.org/10.1016/j.applthermaleng.2011.11.047
[34] Sfriso, S., Berni, F., Fontanesi, S., d'Adamo, A., Breda, S., Teodosio, L., Frigo, S. and Antonelli, M. Combination of G-equation and detailed chemistry: An application to 3D-CFD hydrogen combustion simulations to predict NOx emissions in reciprocating internal combustion engines, *Int. J. Hydrog. Energy*, 2024, **89**, pp 161–176. https://doi.org/10.1016/j.ijhydene.2024.09.252
[35] Simi, A. *Hydrogen direct injection in reciprocating engines using commercial injectors* (Doctoral dissertation). Universit' a di Pisa, 2011.
[36] Fletcher, R.S. and Heywood, J.B. A model for nitric oxide emissions from aircraft gas turbine engines. AIAA Paper No. 71–123, 9th Aerospace Sciences Meeting, New York, NY, January 1971.
[37] Heywood, J.B. and Mikus, T. Parameters controlling nitric oxide emissions from gas turbine combustors. NASA-CR-132959, 1973.
[38] Dederichs, S., Zarzalis, N., Habisreuther, P., Beck, C., Prade, B. and Krebs, W. Assessment of a gas turbine NOx reduction potential based on a spatiotemporal unmixedness parameter, *J. Eng. Gas Turbines Power*, 2013, **135**. https://doi.org/10.1115/1.4025078
[39] Lefebvre, A.H. and Ballal, D.R. *Gas Turbine Combustion: Alternative Fuels and Emissions (3. ed.)*, CRC Press, 2010.
[40] Smith, R. *Advanced low emissions subsonic combustor study: Final report*. NASA Contractor Report NASA/CR-1998-207931, United Technologies Corporation, East Hartford, CT, December 1998.
[41] Pegemanyfar, N. *Development of the preliminary combustor design system PRECODES* (Doctoral dissertation), 2008.
[42] EASA. ICAO aircraft engine emissions databank, 2025. https://www.easa.europa.eu/en/domains/environment/icao-aircraft-engine-emissions-databank
[43] Kurzke, J. *GasTurb 12: Design and off-design performance of gas turbines*, GasTurb GmbH, 2013.
[44] von der Bank, R, et al. *Advances in ultra-high pressure ratio core-engines: Lemcotec preliminary achievements*, Deutscher Luft- und Raumfahrtkongress, 2016.
[45] Schimek, S., Göke, S. and Paschereit, C. Emission formation of liquid fuel combustion under humidified conditions, *51st AIAA Aerospace Sciences Meeting Including the New Horizons Forum and Aerospace Exposition*, 2013. https://doi.org/10.2514/6.2013-693
[46] Hiestermann, M., Konle, M. and Guillebon, L. Numerical investigation of the effect of high steam loads on the combustion of an academic premixed swirl stabilized combustor, 2022. https://doi.org/10.33737/gpps22-tc-94
[47] Göke, S. and Paschereit, C. Influence of steam dilution on NOx formation in premixed natural gas and hydrogen flames, *50th AIAA Aerospace Sciences Meeting Including the New Horizons Forum and Aerospace Exposition*, 2012. https://doi.org/10.2514/6.2012-1272
[48] Riom, E., Larsson, L.-O. and Hagström, U. Verminderung des NOx-Ausstoßes von Dieselmotoren mit dem humid air motorprinzip, *MTZ- Motortechnische Zeitschrift*, 2002, **63**, pp 370–377. https://doi.org/10.1007/BF03227358
[49] Ianniello, R., Pipicelli, M., Di Luca, G., Beatrice, C. and Di Blasio, G. A study on supercritical water injection as waste heat recovery system in internal combustion engines, *Appl. Therm. Eng.*, 2024, **248**, pp 123084. https://doi.org/10.1016/j.applthermaleng.2024.123084
[50] Seitz, A., Nickl, M., Troeltsch, F. and Ebner, K. Initial assessment of a fuel cell—Gas turbine hybrid propulsion concept, *Aerospace*, 2022, **9**, p 68. https://doi.org/10.3390/aerospace9020068
[51] Seitz, A. Propulsion technology options for climate-compliant aircraft design, 2024. https://doi.org/10.5281/zenodo.14946610
[52] Kaiser, S., Schmitz, O., Ziegler, P. and Klingels, H. The water-enhanced turbofan as enabler for climate-neutral aviation, *Appl. Sci.*, 2022, **12**, p 12431. https://doi.org/10.3390/app122312431
[53] Myerson, A.L. The reduction of nitric oxide in simulated combustion effluents by hydrocarbon-oxygen mixtures, *Symposium (International) on Combustion*, 1975, **15**, pp 1085–1092. https://doi.org/10.1016/S0082-0784(75)80373-0
[54] Nicolle, A. and Gagaut, P. Occurrence of NO-reburning in MILD combustion evidenced via chemical kinetic modeling, *Fuel*, 2006, **85**, pp 2469–2478. https://doi.org/10.1016/j.fuel.2006.05.021
[55] Sullivan-Lewis, E., Hack, R. and McDonell, V. Assessment of a rich-burn, quick-mix, lean-burn–Based supplemental burner system in a vitiated air stream, *Combust. Sci. Technol.*, 2016, **188**, pp 397–415. https://doi.org/10.1080/00102202.2015.1119823

Cite this article: Witzgall F., Uhl G., Winter F., Lin Y.-H. and Seitz A. NO_x emission modelling for composite cycle engines with recirculation and water injection: A reduced-order physics-based approach. *The Aeronautical Journal*, https://doi.org/10.1017/aer.2026.10240

https://doi.org/10.1017/aer.2026.10240 Published online by Cambridge University Press